ACS OMEGA

Open Access

http://pubs.acs.org/journal/acsodf

Article

Integrated Network Pharmacology, Molecular Modeling, LC–MS Profiling, and Semisynthetic Approach for the Roots of *Rubia tinctorum* L. Metabolites in Cancer Treatment

Alaa A. El-Banna,[‡‡] Enas E. Eltamany,[‡‡] Asmaa S. A. Yassen, Ahmed Lotfy, Aya H. H. El-Tanahy, Jihan M. Badr,* Mardi M. Algandaby, Samar S. Murshid, Sameh S. Elhady, and Reda F. A. Abdelhameed*

Cite This: *ACS Omega* 2025, 10, 13027−13045

Read Online

ACCESS | Metrics & More | Article Recommendations | Supporting Information

ABSTRACT: *Rubia tinctorum* L. is one of the most widely used plants in folk medicine, with many reported pharmacological activities. One of these valuable activities is its anticancer efficacy. The aim of this study is to explore the multilevel mechanisms of *R. tinctorum* metabolites in cancer treatment using network pharmacology, together with molecular docking and in vitro studies. The network pharmacology analysis enabled us to reveal the hit anticancer *R. tinctorum* constituents, which were found to be acacetin, alizarin, anthragallol, 2-hydroxyanthraquinone, and xanthopurpurin. The most enriched cancer-linked target genes were PLCG1, BCL2, CYP1B1, NSD2, and ESR2. The pathways that were mostly involved in the anticancer mechanism of *R. tinctorum* metabolites were found to be metabolic pathways as well as pathways in cancer and apoptosis. Molecular docking of the identified hit anticancer constituents on the active sites of the most enriched genes unveiled that acacetin and alizarin possessed the lowest binding energies on the active sites of NSD2 and BCL2, respectively. While anthragallol showed the most stabilized interaction on the active sites of PLCG1, CYP1B1, and ESR2. Consequently, *R. tinctorum* extracts were evaluated for their in vitro cytotoxicity on a panel of cancerous cells. Among the tested *R. tinctorum* extracts, the chloroform extract was the strongest one with an IC_{50} = 3.987 μg/mL on the MCF-7 breast cancer cell line. Consequently, it was subjected to chromatographic separation and purification to isolate its major components with reported anticancer activity (scopoletin, rubiadin, chrysophanic acid, alizarin, purpurin, nor-damnacanthal, emodin, and rutin). Alizarin and purpurin constituted the main anthraquinones in *R. tinctorum.* Thus, they were quantified using LC/MS analysis. Moreover, a semisynthetic approach of alizarin toward the enhancement of its anticancer effect on the tested cancer cells was attained. Among the synthesized compounds, 2-methyl alizarin was the most active one with an IC_{50} = 8.878 μg/mL against the HepG2 cell line. This study provides deep insights into the anticancer mechanisms of *R. tinctorum* metabolites for the first time using network pharmacology and valorizes their significance as valuable anticancer agents.

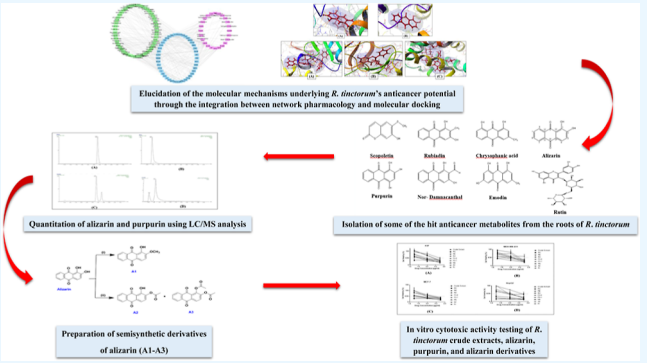

1. INTRODUCTION

Cancer is a serious health problem that is characterized by uncontrollable body cell growth that can pervade throughout the body.[1] It is the second main cause of death globally, behind cardiovascular ailments.[2] In the past decade, there have been 10 million cancer-related deaths and 20 million new instances of cancer worldwide. By 2040, it is anticipated that there will be roughly 30 million additional instances of cancer worldwide, with the largest increases occurring in middle- and low-income nations, if no new steps are taken to control and prevent cancer.[3]

For many years, patients with cancer had only a limited number of treatment options, which included surgery, radiation therapy, and chemotherapy, either individually or in combination.[4] Although these treatment methods were somewhat effective, they exhibited many adverse side effects and problems such as the drug nonselectivity and resistance, in addition to fatigue, hair loss, nausea, vomiting, and pain.[5] Therefore, there was a necessity to improve these treatments and develop new ones with higher safety and efficacy. Recently, various advancements in conventional cancer treatments have been recorded. One of these advancements has been achieved by the

Received: October 29, 2024
Revised: March 9, 2025
Accepted: March 18, 2025
Published: March 26, 2025

Scheme 1. Overview Workflow of the Study

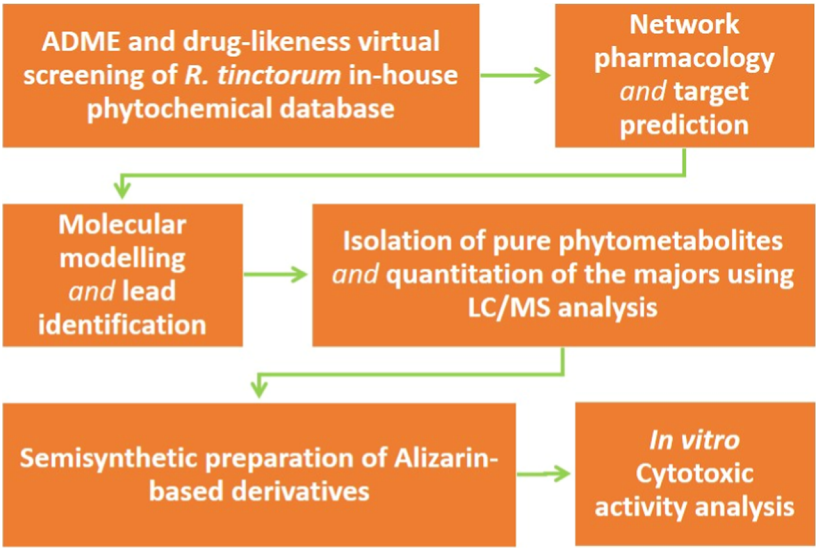

discovery of effective anticancer secondary metabolites from plants and other natural products such as vinca alkaloids, taxanes, epipodophyllotoxins, and derivatives of camptothecin.[6−8] Natural products are still considered to be a wealthy source of promising anticancer agents, and one of these natural products is *Rubia tinctorum* L.

R. tinctorum L., also known as common madder, is a member of the Rubiaceae family. It is indigenous to northern Africa, western Asia, and southern Europe, though it is often cultivated worldwide.[9] Its medicinal part is the dried roots that have a crimson coloring substance that is used as a dye and that gives madder a significant commercial value.[10] The roots are widely used in folk medicine for alleviation of urinary, menstrual, and liver disorders.[9] They are also hired for treatment of bladder and renal stones.[11] Moreover, they are used as a laxative and mild sedative.[12] Many in vitro and in vivo studies have verified the pharmacological activities of *R. tinctorum*. It has been shown to possess anticancer,[13] antioxidant,[14] antimalarial,[12] anti-inflammatory,[15] antifungal,[16] antibacterial,[17] and hepatoprotective[18] activities. These activities are believed to be due to various anthraquinones and their glycosides existing mainly in the roots and rhizomes of *R. tinctorum* such as alizarin, purpurin, pseudopurpurin, purpuroxanthin, ruberythric acid (alizarin-primeveroside), munjistin, rubiadin, nor-damnacanthal, and lucidin primeveroside.[9,12]

Many previous reports have examined the anticancer potential of *R. tinctorum*. For example, Lajkó et al. have emphasized purpurin's efficient and selective ability to inhibit melanoma cells, as well as the potential for its usage as a targeted anticancer treatment.[19] In addition, Rashan et al. have demonstrated that *R. tinctorum* root extracts exhibited antitumor efficiency toward tongue squamous carcinoma and breast cancer cells.[20] Moreover, Abdul Jalill R. has shown that the aqueous root extract of *R. tinctorum* can reduce the cell viability of human glioblastoma cell line (AMGM) with an IC_{50} of 76.44 mg/mL.[21] Furthermore, the anthraquinones, soranjidiol and rubiadin, were found to be effective photochemotherapeutic agents against cancer cells by induction of apoptosis.[22]

Elucidation of natural products' mechanisms in relieving various diseases is very complicated. This is due to natural products' intricate metabolome, the prospective synergism between the metabolites, and their ability to influence many targets simultaneously.[23] This trouble has been successfully solved via the network pharmacology-based analysis that allowed the compound−target gene-disease network to be set up, making it feasible to recognize the multiple targets and pathways of natural product metabolites.[24−29]

The present study's objective is to elucidate the molecular mechanisms underlying *R. tinctorum*'s anticancer potential through the integration between network pharmacology, molecular docking, and in vitro studies for the first time. Isolation of some of the hit anticancer metabolites, their quantitation using LC/MS analysis, and preparation of some of their semisynthetic derivatives to identify their anticancer efficacy were also conducted. The overview workflow of the study is illustrated in Scheme 1. Up to the authors' knowledge, this work represents the first attempt to provide a profound illustration of the anticancer mechanism of *R. tinctorum* metabolites, aiming to valorize them as promising anticancer agents.

2. RESULTS AND DISCUSSION

A database enclosing 67 metabolites (Table S1)[9,12,30−33] was gathered by searching the literature for the phytochemical composition of *R. tinctorum*. Some of these metabolites are common in many plants such as apigenin, luteolin, rutin, and emodin. Therefore, the study in hand focused on the metabolites that are specific to or more abundant in *R. tinctorum* in order to capture the unique bioactivity of the studied plant.

2.1. ADME Filtration of *R. tinctorum* Phytoconstituents. The QikProp module was employed to determine the drug likeness of *R. tinctorum* constituents by evaluating their ADME traits (absorption, distribution, metabolism, and excretion) by measuring certain physicochemical features. The rule of five of Lipinski summed up these physiochemical features. As defined by Lipinski's rule of 5, a chemical with documented biological activity is deemed active if its hydrogen-bond acceptors (Hacc) are less than ten, its hydrogen-bond donors (Hdon) are lower than five, its rotatable bonds are not more than ten, its molecular weight is below 500 Da, and its measured log *P* (*C* log *P*) is not more than five.[34] The database contained only the constituents that fitted with more than two of

https://doi.org/10.1021/acsomega.4c09853
ACS Omega 2025, 10, 13027−13045

the above-mentioned requirements. Furthermore, the database constituents' oral bioavailability (OB) was determined.[35] It estimates the amount of medication taken orally that actually reaches the therapeutic site of action. Compounds having OB < 30% were excluded from the database. All the database compounds complied with the above requirements. Therefore, they were further subjected to network pharmacology analysis. By focusing on drug-likeness criteria, it is aimed to identify compounds that not only exhibit biological activity but also possess favorable pharmacokinetic profiles. This is essential for minimizing the risk of late-stage failures in drug development due to poor absorption, high toxicity, or unfavorable metabolism.[36]

2.2. Finding Out Cancer-Linked Genes of *R. tinctorum* Phytoconstituents by Network Pharmacology-Based Analysis. The results gained from STITCH 5.0 database[37] were utilized to set up a compound−target gene (C−T) network (Figure S1) that allowed for unveiling the cancer-linked genes of *R. tinctorum* constituents. The UniProt[38] and GeneCards[39] databases served to ascertain the job of the identified target genes and how they related to cancer. The STITCH 5.0 database provides "combined scores" for chemical−gene interactions, wherein stronger interactions possess higher scores. Only constituents possessing combined scores ≥0.4 were included in this analysis[28] (Table 1).

The built C−T network (Figure S1) was constituted of 54 nodes (22 compounds and 32 genes) and 363 edges with an average of 3.148 targets for each compound, suggesting the multitarget traits of *R. tinctorum* constituents. The C−T network disclosed that the *R. tinctorum* hit list was comprised mainly of flavonoids and anthraquinones, where acacetin (flavonoid) displayed the highest percentage of C−T interactions (19%), succeeded by alizarin (14%) (anthraquinone), anthragallol (12%) (anthraquinone), 2-hydroxyanthraquinone (12%) (anthraquinone), and xanthopurpurin (12%) (anthraquinone) (Figure 1A).

Papers investigating the role of these hit constituents in cancer were looked up in PubMed to confirm the findings of the network pharmacy analysis (Table S2). For example, acacetin prevented gastric cancer cells from invasively migrating and developing TGF-β1-induced epithelial-to-mesenchymal transition via PI3K/Akt/Snail pathway.[40] It also caused RIP1-dependent necroptotic death and prolonged ERK1/2 activation in breast cancer cells.[41] Moreover, alizarin prevented pancreatic cancer cells from growing by blocking NF-κB activation.[42] It also impaired both breast and bone cancers by inducing cell cycle arrest in the S phase and inhibiting ERK phosphorylation.[43] Furthermore, 2-hydroxyanthraquinone showed a remarkable effect on apoptotic, heat shock, and ER chaperone genes in breast and colon cancer cells. In addition, it induced protein levels of pro-apoptotic pathways, resulting in apoptosis via inhibiting antiapoptotic pathways.[44] It also exhibited inhibitory activity against protein tyrosine kinases v-src and pp60src and arrested the growth of SPC-1-A, Bcap37, and HepG2 cancer cells via the mitochondrial apoptotic pathway.[45] Additionally, xanthopurpurin demonstrated high selective toxicity toward breast and skin cancer cells at lower concentrations without inducing toxicity toward normal cells. Therefore, it can be a promising, safe, and selective anticancer agent.[46] Network pharmacology also disclosed that the most enriched cancer-linked genes that had the highest percentages of C−T interactions were PLCG1 (23%), BCL2 (14%), CYP1B1 (12%), NSD2 (5%), and ESR2 (5%) (Figure 1B). These are renowned cancer-related targets where PLCG1was proved to be essential for the self-renewal of AML1-ETO leukemia stem cells.[47] Moreover, it has been discovered that BCL2 family genes are essential regulators of the induction of apoptosis in various cancer types.[48] Furthermore, CYP1B1 was found to prevent ferroptosis and promote anti-PD-1 resistance in colorectal cancer by breaking down acyl-CoA synthetase long-chain family member 4 (ACSL4).[49] In addition, NSD2 was found to be essential for the proliferation of various human cancer cell types, such as prostate cancer cells, leukemia cells, osteoblastoma cells, and myeloma cells.[50] Also, ESR2 was found to be generally expressed at low levels in breast cancer but associated with improved overall survival and may be related to immune response modulation.[51] Strong associations among the identified cancer-linked genes were observed in the protein−protein network (Figure S2).

Kyoto Encyclopedia of Genes and Genomes (KEGG) pathway analysis was then conducted to assign the functions and pathways of the specified target genes[52] (Table 2 and Figure S3). It disclosed that the specified targets are associated with 37 cancer-linked pathways, where the most significant ones were metabolic pathways, pathways in cancer, and apoptosis that exhibited the largest gene counts and the least false discovery rates (Table 2).

The compound-gene and gene-pathway networks were then merged to set up the compound−target−pathway network (Figure 2) that disclosed robust associations between *R. tinctorum*'s constituents, genes, and pathways.

2.3. Gene Ontology Enrichment Analysis for Targets. DAVID bioinformatics database with the *Homo sapiens* annotation option[53] was hired for conducting gene ontology (GO) enrichment analysis for the network pharmacology-specified targets. It allowed for the identification of the most significant pathways and GO terms (cellular components, biological processes, and molecular functions) with the highest log *p*-values and gene counts. Figure 3A demonstrates the involvement of 2 BIOCARTA pathways, which are apoptotic signaling in response to DNA damage and cell cycle and 37 KEGG pathways enclosing the NF-kappa B signaling pathway, pathways in cancer, and chemical carcinogenesis. The adjusted *P*-value for each of these determined pathways was ≤0.01 (*P*-values were corrected using the Benjamini−Hochberg method[54] to minimize false positives), proving their significant correlation with cancer.

Figure 3B unveils that the most important biological processes were negative regulation of the apoptotic process and long-chain fatty acid biosynthetic process, while the most enriched molecular functions were heme binding and enzyme binding. Meanwhile, the most significant cellular components were cytosol and cytoplasm.

2.4. Molecular Docking of *R. tinctorum* Hit Constituents on the Binding Sites of the Most Enriched Cancer-Linked Target Genes. Molecular docking simulations were performed in this study to elucidate the binding interactions between the most enriched target proteins and potential drug candidates (hit compounds) identified from the network pharmacology analysis, thereby providing insights into their affinity and specificity. The basic principle of molecular docking involves predicting the optimal binding orientation and energy of small molecules within the active site of the receptor, thereby facilitating the identification of promising candidates for further development in the drug discovery process.[55]

https://doi.org/10.1021/acsomega.4c09853
ACS Omega 2025, 10, 13027−13045

Table 1. Target Proteins for *R. tinctorum* Constituents

	short name of protein	full name of protein	interacting compound (s) (combined interaction score)
1	AKR1B1	aldo-keto reductase family 1 member B1	acacetin (0.68)
2	AKR1B10	aldo-keto reductase family 1 member B10	acacetin (0.74)
3	ALOX5	arachidonate 5-lipoxygenase	acacetin (0.67)
4	APAF1	apoptotic protease-activating factor 1	2-hydroxy anthraquinone (0.48), 2-methoxyanthraquinone (0.44)
5	APEX1	DNA-(apurinic or apyrimidinic site) lyase	alizarin 1-methyl ether (0.4), alizarin 2-methyl ether (0.4)
6	APP	amyloid-beta precursor protein	acacetin (0.67)
7	BCL2	apoptosis regulator Bcl-2	anthragallol (1), alizarin (1), xanthopurpurin (1)
8	BCL2A1	Bcl-2-related protein A1	munjistin (0.4), anthragallol (0.41), rubiadin (0.41), lucidin (0.4)
9	CBS	cystathionine beta-synthase	acacetin (0.73)
10	CDC25B	M-phase inducer phosphatase 2	pseudopurpurin (0.41), 2-hydroxyanthraquinone (0.57), 2-methoxyanthraquinone (0.5)
11	CDK9	cyclin-dependent kinase 9	acacetin (1)
12	CREB1	cyclic AMP-responsive element-binding protein 1	acacetin (0.53)
13	CYP1A1	cytochrome P450 1A1	acacetin (0.48)
14	CYP1A2	cytochrome P450 1A2	acacetin (1)
15	CYP1B1	cytochrome P450 1B1	purpurin (1), alizarin (1), alizarin 1,2-dimethylether (0.44), acacetin (1), anthragallol 3-methyl ether (0.5), alizarin 2-methyl ether (0.61), xanthopurpurin-3-methyl ether (0.5), xanthopurpurin-1-methyl ether (0.42), anthragallol-2,3-dimethyl ether (0.47)
16	CYP27A1	sterol 26-hydroxylase, mitochondrial	2-methoxyanthraquinone(0.42)
17	CYP2C19	cytochrome P450 2C19	acacetin (1)
18	CYP3A4	cytochrome P450 3A4	acacetin (1)
19	ERN1	serine/threonine-protein kinase/endoribonuclease IRE1	anthragallol 3-methyl ether (0.43), xanthopurpurin-1-methyl ether (0.4), alizarin 2-methyl ether (0.43)
20	ESR1	estrogen receptor	2-hydroxyanthraquinone (0.86), 7-hydroxy-2-methylanthraquinone (0.75)
21	ESR2	estrogen receptor beta	acacetin (0.74), 2-hydroxyanthraquinone (0.86), 7-hydroxy-2-methylanthraquinone (0.75)
22	GAPDH	glyceraldehyde-3-phosphate dehydrogenase	2-methoxyanthraquinone (0.47)
23	IL2	interleukin-2	acacetin (0.44)
24	MALT1	mucosa-associated lymphoid tissue lymphoma translocation protein 1	2-methoxyanthraquinone (0.44)
25	MCL1	induced myeloid leukemia cell differentiation protein Mcl-1	anthragallol (1), alizarin (1), xanthopurpurin (1)
26	NSD2	histone-lysine *N*-methyltransferase NSD2	alizarin (0.44), 2-hydroxyanthraquinone (0.48), rubiadin (0.43), 1-hydroxy-2-methylanthraquinone (0.46), alizarin 1-methyl ether (0.43), alizarin 2-methyl ether (0.42), alizarin 1,2-dimethyl ether (0.43), 1-methoxy-2-methyl-anthraquinone (0.43), 2-methoxyanthraquinone (0.5)
27	PGF	placenta growth factor	acacetin (0.55)
28	PLCG1	1-phosphatidylinositol 4,5-bisphosphate phosphodiesterase gamma-1	purpurin (0.42), alizarin (0.42), xanthopurpurin (0.41), anthragallol (0.41), 2-hydroxyanthraquinone (0.48)
29	PTPN13	tyrosine-protein phosphatase nonreceptor type 13	2-hydroxyanthraquinone (0.48), 2-methoxyanthraquinone (0.44)
30	PTPRC	receptor-type tyrosine-protein phosphatase C	pseudopurpurin (0.46), munjistin (0.45), anthragallol (0.41), purpurin (0.42), alizarin (0.42), xanthopurpurin (0.41), 2-hydroxyanthraquinone (0.54), 2-methoxyanthraquinone (0.44), alizarin 2-methyl ether (0.45), alizarin 1,2-dimethyl ether (0.46), anthragallol 3-methyl ether (0.44), xanthopurpurin-1-methyl ether (0.44), anthragallol-2,3-dimethyl ether (0.42), xanthopurpurin dimethyl ether (0.45)

https://doi.org/10.1021/acsomega.4c09853
ACS Omega 2025, 10, 13027−13045

Table 1. continued

	short name of protein	full name of protein	interacting compound (s) (combined interaction score)
31	SMAD3	mothers against decapentaplegic homologue 3	2-hydroxyanthraquinone (0.48), 2-methoxyanthraquinone (0.44)
32	XDH	xanthine dehydrogenase/oxidase	acacetin (0.74)

The most enriched genes recognized from network pharmacology analysis were 1-phosphatidylinositol 4,5-bisphosphate phosphodiesterase gamma-1, apoptosis regulator B-cell lymphoma 2 (Bcl-2), cytochrome P450 1B1, histone-lysine *N*-methyltransferase NSD2, and estrogen receptor beta.

1-Phosphatidylinositol 4,5-bisphosphate phosphodiesterase gamma-1 (PLCγ1) is a member of the phospholipase C family. It consists of two central catalytic domains forming the triose phosphate isomerase (TIM) α/β barrel (X- Y- box) and noncatalytic domains—a pleckstrin homology (PH), EF-hand, and a C2 domain. The two catalytic domains are separated from each other by the specific array (SA), which consists of a split PH (spPH) domain that is separated by two SH2 domains (nSH2 and cSH2), an SH3 domain, and an intervening linker that contains a crucial tyrosine residue, Y783. Physiological PLCγ1 activation occurs following its recruitment to receptor or nonreceptor tyrosine kinases (RTKs and TKs), which in turn phosphorylate the PLCγ1 SA domain on tyrosine residue 783. Either the aminoterminal nSH2 domain or the carboxyterminal cSH2 domain has been found to bind to an activated RTK. Activation of PLCγ1 occurs due to the intramolecular binding of the phosphorylated Y783 to the cSH2 domain, which leads to conformational changes in the protein and the release of the cSH2 domain from the catalytic core of PLCγ1.[56]

Bcl-2 is a key regulator of apoptosis and belongs to a family of proteins that either promote or inhibit apoptosis. It contains four Bcl-2 homology (BH) domains designated as BH1, BH2, BH3, and BH4. These domains are crucial for its function in regulating apoptosis. It also has a hydrophobic C-terminal region that anchors it to the mitochondrial membrane, where it exerts its protective effects against apoptosis. The protein predominantly consists of α-helical structures, which play a significant role in its interactions with other proteins. Bcl-2 exhibits conformational flexibility, which allows it to interact with various pro-apoptotic proteins such as Bax and Bak. This flexibility is essential for its ability to sequester these proteins and inhibit their pro-apoptotic functions. It can also form homodimers and heterodimers with other Bcl-2 family members. The dimerization process is influenced by the binding of ligands and the presence of other interacting proteins. The BH3 domain of pro-apoptotic proteins binds to the BH1 and BH2 domains of Bcl-2, inhibiting its function. This pocket is critical for the regulation of apoptosis.[57] Moreover, cytochrome P450 1B1 (CYP1B1) is an enzyme belonging to the cytochrome P450 superfamily, which is involved in the metabolism of various substrates. It contains a heme prosthetic group that is crucial for its enzymatic activity. The iron within the heme plays a vital role in the oxidation−reduction reactions. The enzyme has a hydrophobic region that anchors it to the endoplasmic reticulum membrane, allowing it to interact with various substrates and electron donors. It also has specific cavities and pockets that facilitate substrate binding and recognition, characterized by distinct amino acid residues. There is a characteristic distortion of helix F where $\pi-\pi$ stacking interactions occur with Phe231. The amino acid residuesVal395 and Ala133 determine the cavity shape in the vicinity of the heme.[58,59] The enzyme undergoes significant conformational changes during the binding and metabolism of substrates, which can include the opening and closing of access channels to the active site.[58] Furthermore, histone-lysine *N*-methyltransferase NSD2 is an important enzyme involved in epigenetic regulation through the methylation of histones. It contains an SET domain, which is characteristic of methyltransferases. This domain is responsible

https://doi.org/10.1021/acsomega.4c09853
ACS Omega 2025, 10, 13027−13045

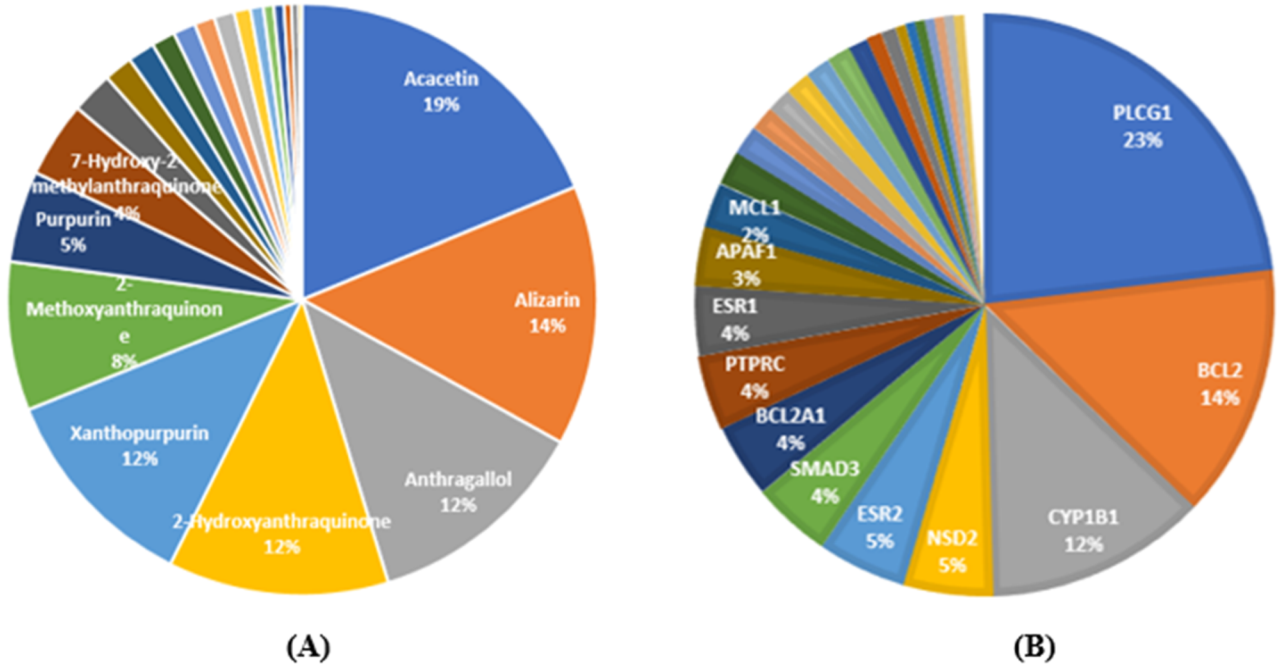

Figure 1. Distributions % of the compound−target gene (C−T) interactions on *R. tinctorum* constituents (A) and the identified cancer-related genes (B).

for transferring methyl groups to lysine residues on histones. It also has multiple zinc finger motifs that play a role in protein−protein interactions and may contribute to its stability and specificity. In addition, the enzyme features a catalytic cavity, where the substrate (histone lysine) binds and undergoes methylation. It also includes flexible loops that can adopt different conformations, influencing their interaction with substrates and inhibitors. NSD2 requires *S*-adenosylmethionine (SAM) as a methyl donor, and the binding site for SAM is crucial for its methyltransferase activity.[60] Additionally, estrogen receptor β is a nuclear hormone receptor that plays a crucial role in mediating the effects of estrogen in various tissues. It contains a DNA-binding domain (DBD) with a zinc finger structure that allows it to bind to specific estrogen response elements in DNA. It also has a ligand-binding domain (LBD) that is responsible for binding estrogen and is critical for receptor activation. It has a hydrophobic pocket that accommodates the ligand. The protein contains transactivation domain that is involved in recruiting coactivators and transcriptional machinery to initiate gene expression. In addition, it has a flexible hinge region that connects the DBD and LBD and plays a role in receptor dimerization and conformational changes.[61]

In this study, three crystal structures were selected from RCSB Protein Data Bank (PDB) (https://www.rcsb.org/) for each of the most enriched targets related to cancer identified from network pharmacology analysis. Following that, the three crystal structures of each protein were compared using two procedures: the first is the redocking procedure in which the cocrystallized ligands were docked back into the receptor binding cavity. Prior to performing the redocking experiments, the ligands were converted to SMILES format before converting them back to 3D structures in order to lose the binding coordinates, allowing for a more reliable evaluation of the docking accuracy. After performing the redocking experiments, the relative mean standard deviation (RMSD) value between the initial conformation and the redocked one was calculated for each crystal structure. The lower the (RMSD) value, the higher the accuracy of docking pose prediction.[62,63] The second procedure is the enrichment calculations that are crucial for evaluating the ability of the virtual screening software to find the active ligands throughout the background database in a random selection of ligands.[62,63] In this procedure, a validation set composed of active compounds for each of the studied proteins was seeded into 1000 built-in Schrodinger decoys (Table S3). Decoys are compounds that are similar in physical properties with respect to the reference ligand that might not bind effectively to a protein.[64] Validation parameters such as area under curve of receiver operating characteristic (AUC-ROC), enrichment factor (EF at 2%, 5%, and 10%), and BEDROC were then estimated. From the ROC plots, the area under the curve (AUC) computed the probability of how highly a randomly selected active is ranked compared to a randomly chosen decoy. The ideal range of AUC is 0−1, a value near $\leq$0.5 indicates that the software randomly selects true actives and false actives, where a value close to 1 highlights greater possibility to identify true actives before false ones.[65] Comparing EF values revealed that the investigated proteins were able to extract actives from a seeded random set, when the top 2, 5, and 10% of the total set were considered, noting that the maximum attainable enrichment factors are 50, 20, and 10 for EF(2%), EF(5%), and EF(10%), respectively.[66] However, BEDROC is a criteria used to assess early recognition of actives from decoys at different tuning parameter values α.[67] The crystal structure displaying the lowest RMSD and the best enrichment values for each protein was chosen for molecular docking with *R. tinctorum*'s hit phytoconstituents (Table S4).

The selected crystal structures were PDB ID: 7NXE for 1-phosphatidylinositol 4,5-bisphosphate phosphodiesterase gamma-1, PDB ID: 2Y6W for apoptosis regulator Bcl-2, PDB ID: 6IQ5 for cytochrome P450 1B1, PDB ID: 7VLN for histone-lysine *N*-methyltransferase NSD2, and PDB ID: 2GIU for estrogen receptor beta.

In this study, the Schrodinger suite software's Glide module was employed to compute the XP G scores of *R. tinctorum* hit

https://doi.org/10.1021/acsomega.4c09853
ACS Omega 2025, 10, 13027−13045

Table 2. KEGG Pathway Analysis of the Identified Target Genes

pathway ID	pathway description	observed gene count	false discovery rate	matching proteins in network
hsa01100	metabolic pathways	13	1.37×10^{-6}	AKR1B1, AKR1B10, ALOX5, CBS, CYP1A1, CYP1A2, CYP27A1, CYP2C19, CYP3A4, GAPDH, NSD2, PLCG1, XDH
hsa05200	pathways in cancer	8	1.47×10^{-9}	APAF1, BCL2, ESR1, ESR2, IL2, PGF, PLCG1, SMAD3
hsa04210	apoptosis	6	1.16×10^{-5}	APAF1, BCL2, BCL2A1, ERN1, MCL1, PTPN13
hsa05204	chemical carcinogenesis	5	1.02×10^{-6}	CYP1A1, CYP1A2, CYP1B1, CYP2C19, CYP3A4
hsa05206	microRNAs in cancer	5	3.64×10^{-6}	BCL2, CDC25B, CYP1B1, MCL1, PLCG1
hsa04151	PI3K-Akt signaling pathway	5	6.05×10^{-5}	BCL2, CREB1, IL2, MCL1, PGF
hsa04915	estrogen signaling pathway	4	0.00012	BCL2, CEB1, ESR1, ESR2
hsa04064	NF-kappa B signaling pathway	4	8.16×10^{-10}	BCL2, BCL2A1, MALT1, PLCG1
hsa00140	steroid hormone biosynthesis	4	6.05×10^{-5}	CYP1A1, CYP1A2, CYP1B1, CYP3A4
hsa00982	drug metabolism—cytochrome P450	3	0.001	CYP1A2, CYP2C19, CYP3A4
hsa01522	endocrine resistance	3	0.00034	BCL2, ESR1, ESR2
hsa04066	HIF-1 signaling pathway	3	0.0288	BCL2, GABDH, PLCG1
hsa05166	human T-cell leukemia virus 1 infection	3	0.0291	CERB1, IL2, SMAD3
hsa04913	ovarian steroidogenesis	3	3.13×10^{-5}	ALO5, CYP1A1, CYP1B1
hsa04659	Th17 cell differentiation	3	0.027	IL2, SMAD3, PLCG1
hsa05202	transcriptional misregulation in cancer	3	0.00038	BCL2A1, CDK9, NSD2
hsa00380	tryptophan metabolism	3	0.0037	CYP1A1, CYP1A2, CYP1B1
hsa00590	arachidonic acid metabolism	2	6.05×10^{-5}	ALOX5, CYP2C19
hsa05224	breast cancer	2	0.0124	ESR1, ESR2
hsa04110	cell cycle	2	0.0065	CDC25B, SMAD3
hsa05210	colorectal cancer	2	0.0185	BCL2, SMAD3
hsa04625	C-type lectin receptor signaling pathway	2	0.0037	IL2, MALT1
hsa00983	drug metabolism—other enzymes	2	0.0153	CYP3A4, XDH
hsa01521	EGFR tyrosine kinase inhibitor resistance	2	0.0166	BCL2, PLCG1
hsa04666	Fc gamma R-mediated phagocytosis	2	0.0234	PLCG1, PTPRC
hsa00790	folate biosynthesis	2	0.0234	AKR1B1, AKR1B10
hsa05226	gastric cancer	2	0.0124	BCL2, SMAD3
hsa04935	growth hormone synthesis, secretion and action	2	0.0343	CREB1, PLCG1
hsa05225	hepatocellular carcinoma	2	0.0024	PLCG1, SMAD3
hsa04722	neurotrophin signaling pathway	2	0.0315	BCL2, PLCG1
hsa04115	p53 signaling pathway	2	0.0145	APAF1, BCL2
hsa05020	prion disease	2	0.0025	APAF1, CREB1
hsa04917	prolactin signaling pathway	2	0.0127	ESR1, ESR2
hsa05215	prostate cancer	2	0.00035	BCL2, CREB1
hsa05205	proteoglycans in cancer	2	0.0246	ESR1, PLCG1
hsa05222	small cell lung cancer	2	0.0027	APAF1, BCL2
hsa04919	thyroid hormone signaling pathway	2	0.0362	ESR1, PLCG1

constituents, acacetin, alizarin, anthragallol, hydroxyanthraquinone, and xanthopurpurin, on the active sites of the most enriched targets related to cancer: PLCG1, BCL2, CYP1B1, NSD2, and ESR2. Table 3 discloses that anthragallol possessed the least XP G score upon binding with 1-phosphatidylinositol 4,5-bisphosphate phosphodiesterase gamma-1, cytochrome P450 1B1, and estrogen receptor beta, whereas alizarin demonstrated the most stable interaction with the apoptosis regulator Bcl-2. Meanwhile, acacetin exhibited the lowest binding energy with histone-lysine *N*-methyltransferase NSD2.

The 2D and 3D diagrams of anthragallol's interaction with 1-phosphatidylinositol 4,5-bisphosphate phosphodiesterase gamma-1 active site (Figure 4A) showed the formation of a hydrogen bond between C2 hydroxyl group and Thr590 and other three hydrogen bonds between C3 hydroxyl group and Thr596, Arg586, and Ser588 residues. There were also hydrophobic interactions with Phe591 and Cys608; in addition to charged positive interactions with Arg562, Arg609, Arg586, and Arg559; charged negative interaction with Glu589; and polar interactions with Thr590, Thr596, Ser588, and Hie607.[68]

The stable binding of anthragallol on the active site of cytochrome P450 1B1was found to be due to the formation of a hydrogen bond between the C3 hydroxyl group and Ile462, in addition to another hydrogen bond between the C10 ketone group and Arg117. Moreover, hydrophobic interactions with Ile399, Ile462, Val395, Phe463, Ala330, Cys470, Ala133, Ile471, Met132, and Trp141; charged positive interactions with Arg145,

https://doi.org/10.1021/acsomega.4c09853
ACS Omega 2025, 10, 13027−13045

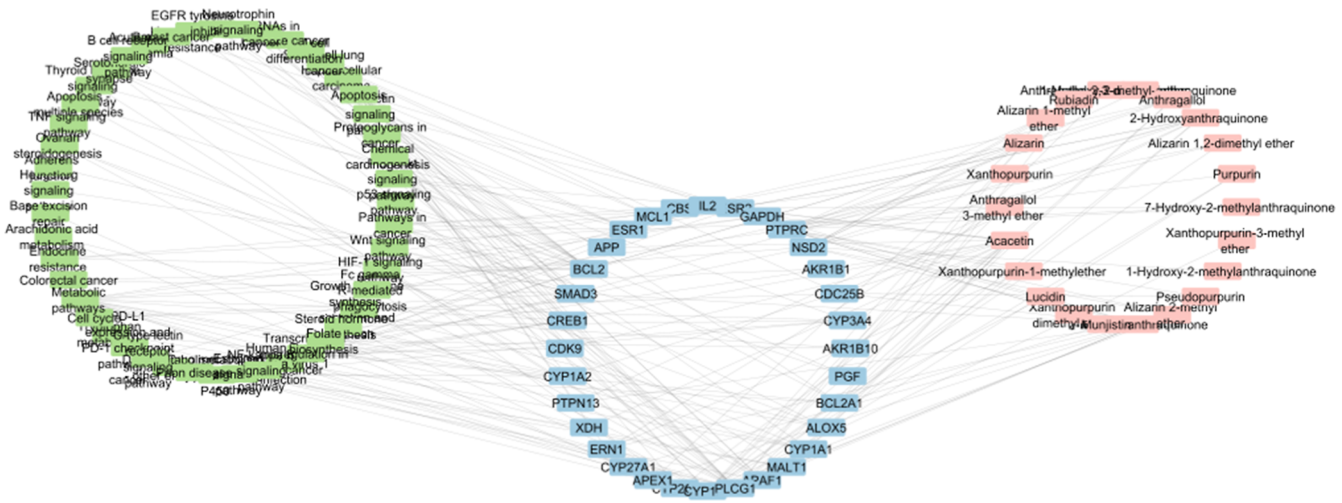

Figure 2. Compound−target−pathway network (compounds are represented in purple color, targets are presented in blue color, and pathways are presented in green color).

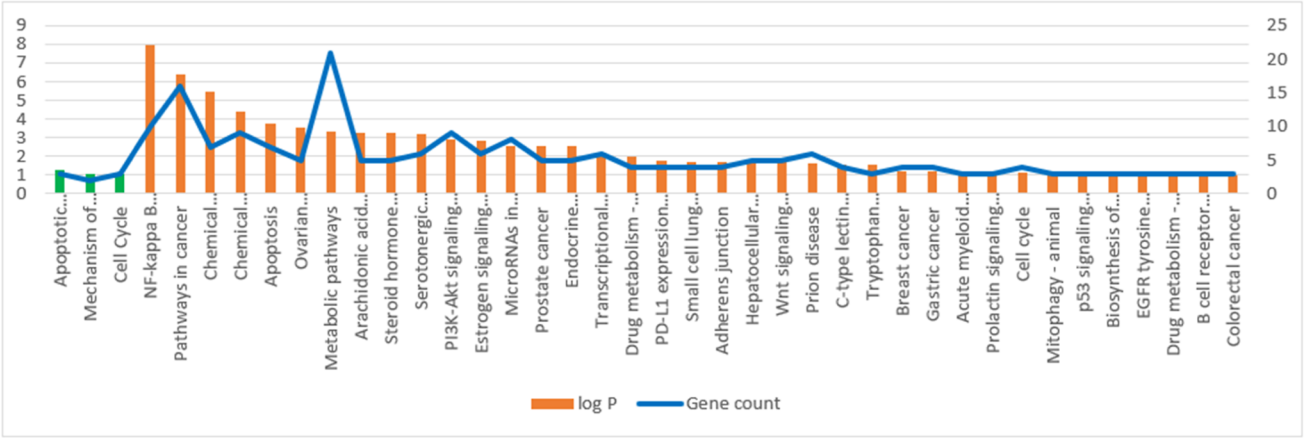

(A)

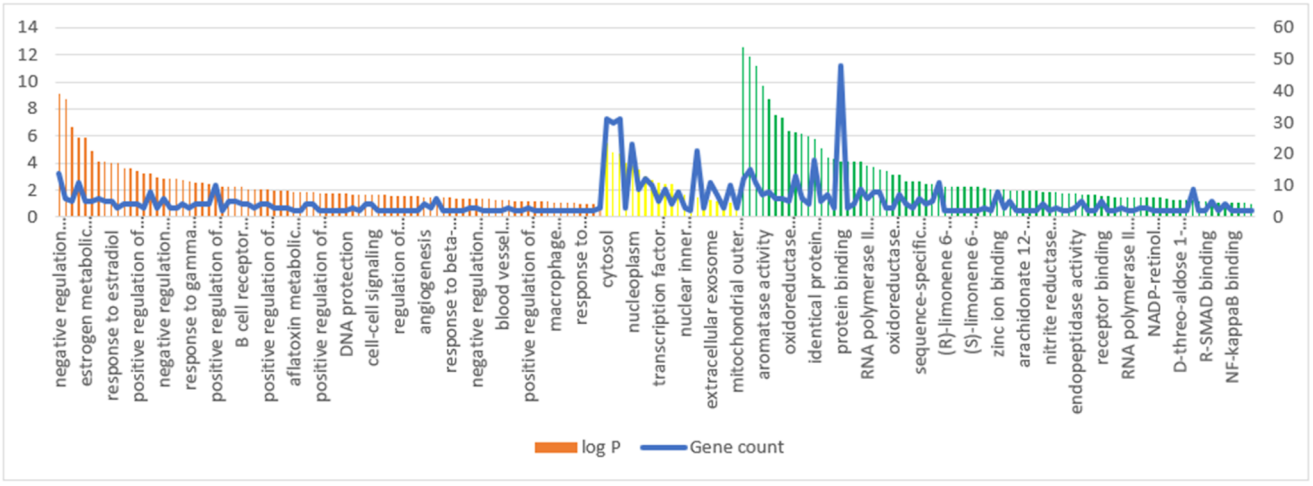

(B)

Figure 3. BIOCARTA (green) and KEGG (orange) pathways involved in cancer and generated by DAVID database (A). GO enrichment analysis of identified cancer targets. Biological processes are colored orange, cellular components are yellow, and molecular functions are green (B). The order of importance was ranked by −log 10 (adjusted *P*-value) with a bar chart. The number of targets stick into each term with a line chart.

Arg468, and Arg117; and polar interactions with Thr398, Ser464, Gln424, and Thr334 were also observed[69] (Figure 4B).

Furthermore, anthragallol was stabilized in the active site of estrogen receptor beta through a pair of hydrogen bonds between C1 and C2 hydroxyl groups and Glu305, and another

https://doi.org/10.1021/acsomega.4c09853
ACS Omega 2025, 10, 13027−13045

Table 3. XP G Scores of the Top Hit *R. tinctorum* Constituents against the Most Enriched Cancer-Linked Target Proteins

	1-phosphatidylinositol 4,5-bisphosphate phosphodiesterase gamma-1 (7NXE)	apoptosis regulator Bcl-2 (2Y6W)	cytochrome P450 1B1 (6IQ5)	histone-lysine *N*-methyltransferase NSD2 (7VLN)	estrogen receptor beta (2GIU)
acacetin	−4.508	−5.326	−5.036	−7.533	−7.782
alizarin	−4.431	−6.595	−7.024	−6.74	−9.436
anthragallol	−5.814	−6.125	−7.865	−6.744	−9.514
hydroxyanthraquinone	−3.753	−5.325	−5.211	−5.559	−8.705
xanthopurpurin	−5.321	−6.188	−7.092	−5.545	−8.854

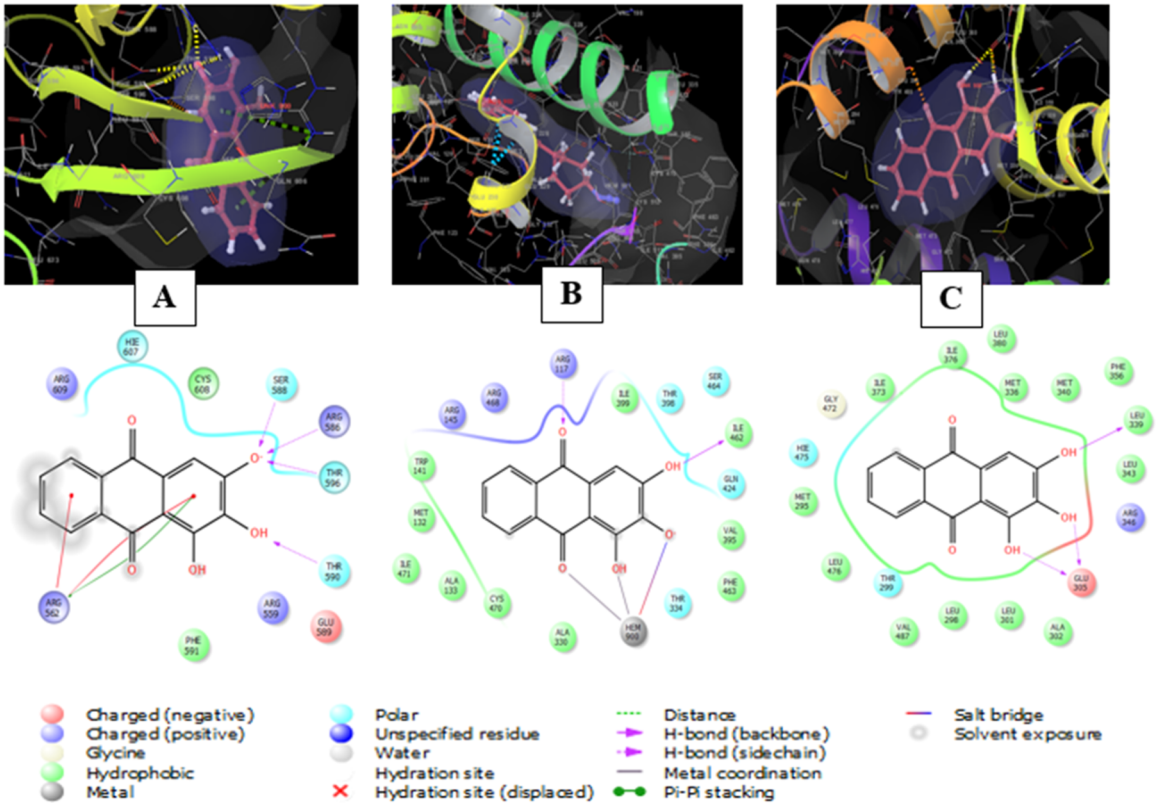

Figure 4. 2D and 3D interaction diagrams of (A) anthragallol in the active site of 1-phosphatidylinositol 4,5-bisphosphate phosphodiesterase gamma-1 (PDB ID 7NXE); (B) anthragallol in the active site of cytochrome P450 1B1 (PDB ID 6IQ5); and (C) anthragallol in the active site of estrogen receptor beta (PDB ID 2GIU).

hydrogen bond was formed between C3 hydroxyl group and Leu339. In addition, there were hydrophobic interactions with Ile373, Ile376, Leu380, Met336, Met340, Phe356, Leu339, Leu343, Ala302, Leu301, Leu298, Val487, Leu476, and Met295; a charged positive interaction with Arg346; a charged negative interaction with Glu 305; and polar interactions with Thr299 and Hie475[70] (Figure 4C).

On the other hand, alizarin occupied the apoptosis regulator Bcl-2's binding site via hydrophobic interactions with PheB 57, AlaA 105, PheA 102, AlaA 98, ValA 101, PheA 53, ValB 101, and PheB 53 and a charged negative interaction with GluB 54[71] (Figure 5A).

Furthermore, the binding of acacetin with histone-lysine *N*-methyltransferase NSD2 involved a hydrogen bond between 7 hydroxyl group and Asp269; pi−pi stacking interactions between the aromatic ring B of the flavonol moiety and Tyr233 and Trp236; hydrophobic interactions with Tyr233, Leu318, Val230, Trp235, Pro234, Trp236, Phe266, Phe267, and Ala270; a charged positive interaction with Lys229; charged negative interactions with Glu272 and Asp269; and polar interactions with Ser228 and Gln321[72] (Figure 5B).

For providing more accurate estimation of ligand−target binding interactions, we incorporated the Molecular Mechanics/Generalized Born Surface Area (MM_GBSA) binding energy calculations to account for simulated solvation entropy and evaluate the nature of interaction based on different energy terms.[73] The FastDRH free online platform (http://cadd.zju.edu.cn/fastdrh/overview) has been adopted to predict and analyze the ligand−target binding interactions based on MM_GBSA decompositions.[74] Pose rescoring of the top-docked compound−protein complexes was proceeded through Amber protein force fields and under explicit water model (nonpolarizable four-point rigid optimal point charge; OPC) solvation conditions being reported with better performance over other force field and water models.[74,75] Interestingly, electrostatic interactions (ELE) have been assigned with dominant contributions over van der Waals (VDW) potentials within the binding energies of all investigated complexes, except that of BCL2-alizarin complex where electrostatic interactions were inferior (Table 4). The latter highlights the advent of polar functionalities within the chemical structures of investigated compounds to ensure ligand stability within the target pocket

https://doi.org/10.1021/acsomega.4c09853
ACS Omega 2025, 10, 13027−13045

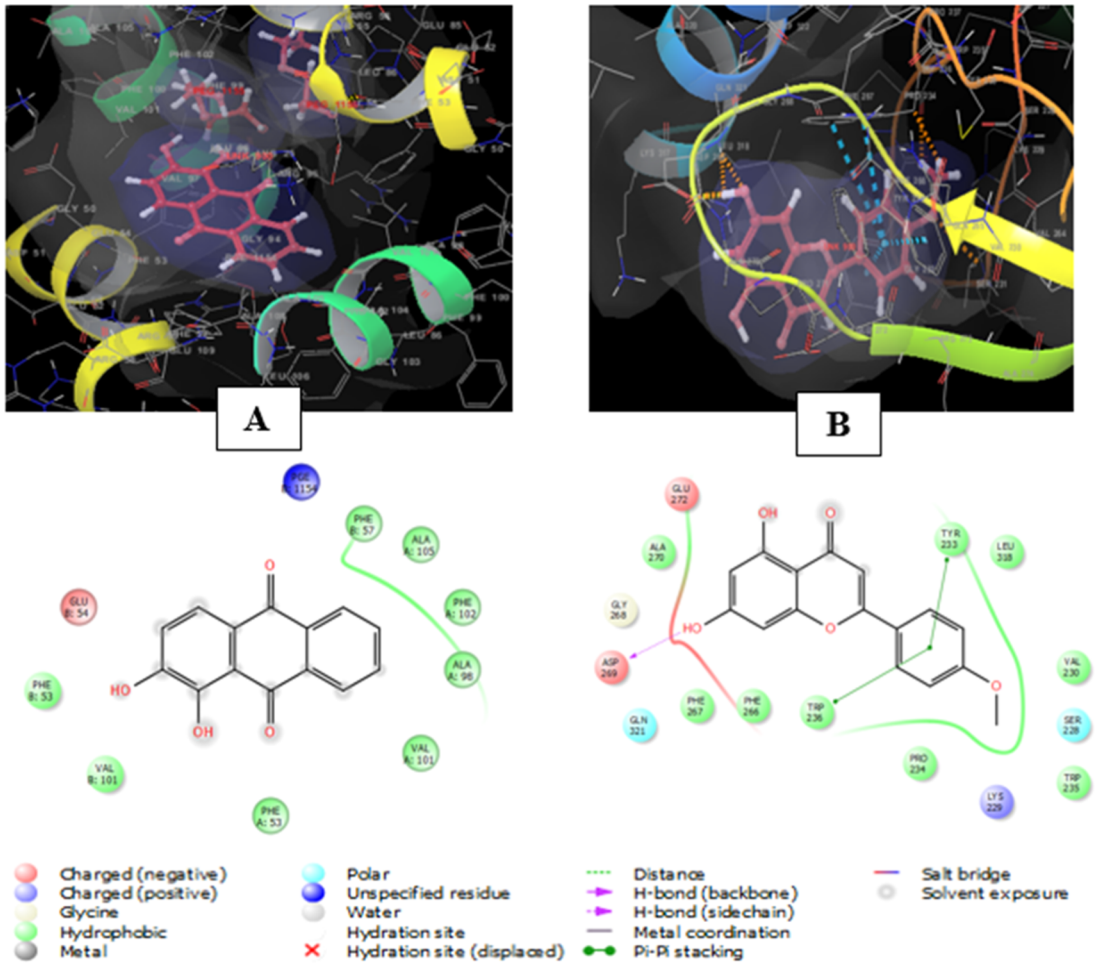

Figure 5. 2D and 3D interaction diagrams of (A) alizarin in the active site of the apoptosis regulator Bcl-2 (PDB ID 2Y6W); (B) acacetin in the active site of histone-lysine *N*-methyltransferase NSD2 (PDB ID 7VLN).

Table 4. MM_GBSA Binding Energy Calculations and Dissected Contribution Energy Terms (kcal/mol)[a] of the Top-Docked Compound−Target Complexes

	PLCG1-anthragallol complex	BCL2-alizarin complex	CYP1B1-anthragallol complex	NSD2-acacetin complex	ESR2-anthragallol complex
ELE	−117.19	−13.95	−139.32	−48.04	−47.63
VDW	−14.58	−29.34	−33.76	−29.9	−27.52
INT	0.01	0	0.01	−0.01	0
GAS	−131.76	−43.29	−173.07	−77.95	−75.15
GBSUR	−2.98	−2.29	−4.13	−4.88	−3.33
GB	113.2	21.66	143.88	50.02	32.42
GBSOL	110.22	19.37	139.75	45.14	29.09
GBELE	−3.99	7.71	4.56	1.98	−15.21
GBTOT	−21.54	−23.92	−33.32	−32.81	−46.06

[a]ELE = electrostatic interactions; VDW = van der Waals interactions between the fragments; INT = internal energy arising from bond, angle, and dihedral terms in the MM force field; GAS = total gas phase energy (ELE + VDW + INT); GBSUR = nonpolar contribution to solvation; GB = electrostatic contribution to the solvation free energy; GBSOL = sum of nonpolar and polar contributions to solvation (GBSUR + GB); GBELE = sum of the electrostatic solvation free energy and MM electrostatic energy (ELE + GB); and GBTOT = estimated total binding free energy calculated from the terms above (GAS + GBSOL).

sites. Nonetheless, electrostatic contributions could be considered a double-bladed knife as their contribution to the solvation free energy (GB) was the highest for anthragallol at both PLCG1 and CYP1B1 complexes, conferring a compromised binding process since the later has been considered a solvent-displacement process.[76,77]

Thus, it is suggested that further lead compound development through the introduction of functional group of balanced hydrophobic/polar characteristics (e.g., tetrazoles and other carboxylate bioisosteres) would be beneficial for optimizing the compound−target complex stability and in turn the biological activity.[78]

2.5. Structure Elucidation of Some of the Hit Anticancer Metabolites from the Roots of *R. tinctorum*.

2.5.1. Spectroscopic Data of the Isolated Compounds (2−7).

2.5.1.1. Rubiadin (2). Yellow powder; ^{1}H NMR (400 MHz,

https://doi.org/10.1021/acsomega.4c09853
ACS Omega 2025, 10, 13027−13045

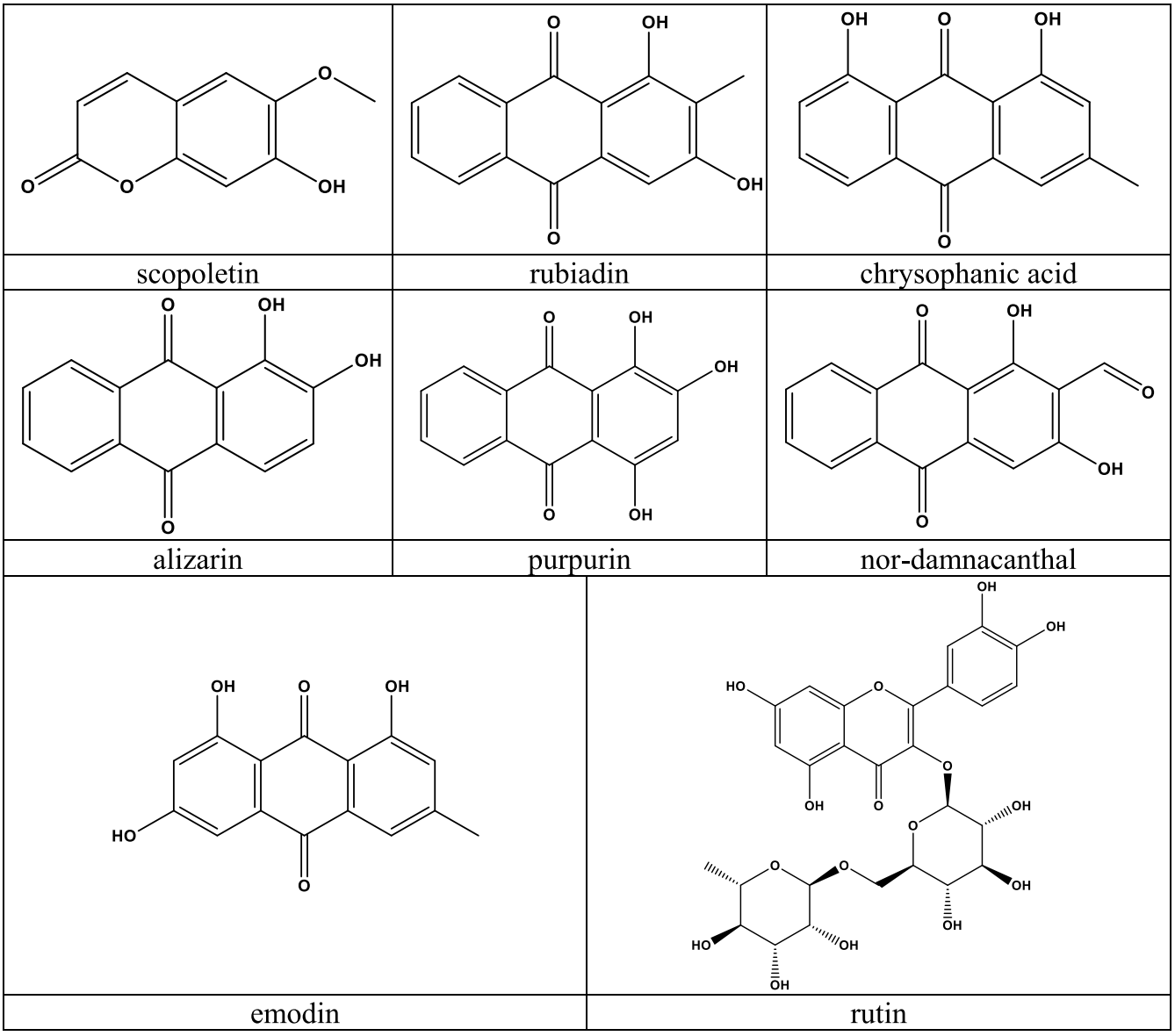

Figure 6. Chemical structures of the hit anticancer constituents isolated from *R. tinctorum* L.

DMSO-d_6): δ H 7.30, s (H-4), 8.12, br.d, J = 8 (H-5), 7.69, m (H-6&7), 8.20, br.d, J = 8 (H-8), 2.12, s (CH_3). ^{13}C NMR (100 MHz, DMSO-d_6): δ C 162.4 (C-1), 117.3 (C-2), 162.8 (C-3), 107.3 (C-4), 126.3 (C-5), 134.4 (C-6), 134.5 (C-7), 126.7 (C-8), 186.2 (C-9), 181.8 (C-10), 133.0 (C-11), 132.9 (C-12), 108.9 (C-13), 131.7 (C-14), 8.07 (CH_3).

*2.5.1.2. Chrysophanic Acid (**3**).* Yellow powder; ^{1}H NMR (600 MHz, $CDCl_3$): δ H 7.04, d, J = 1.2 (H-2), 7.59, d, J = 1.2 (H-4), 7.76, dd, J = 1.2, 7.8 (H-5), 7.60, t, J = 7.8 (H-6), 7.23, dd, J = 1.2, 8.4 (H-7), 2.40, s (CH_3), 11.95, s (C1−OH), 12.06, s (C8−OH). ^{13}C NMR (150 MHz, $CDCl_3$): δ C 162.7 (C-1), 124.4 (C-2), 149.3 (C-3), 121.4 (C-4), 119.9 (C-5), 137.0 (C-6), 124.6 (C-7), 162.4 (C-8), 192.6 (C-9), 182.0 (C-10), 115.9 (C-11), 109.0 (C-12), 113.7 (C-13), 133.6 (C-14), 22.3 (CH_3).

*2.5.1.3. Alizarin (**4**).* Violet powder; ^{1}H NMR (400 MHz, DMSO-d_6): δ H 6.35, d, J = 8 (H-3), 6.58, d, J = 8 (H-4), (7.41−7.47, m) (H-5&8), 6.93−6.99, m (H-6&7). ^{13}C NMR (100 MHz, DMSO-d_6): δ C 152.7 (C-1), 150.7 (C-2), 121.0 (C-3), 120.7 (C-4), 126.7 (C-5), 135.0 (C-6), 134.0 (C-7), 126.4 (C-8), 188.6 (C-9), 180.4 (C-10), 132.7 (C-11), 133.5 (C-12), 116.1 (C-13), 123.7 (C-14).

*2.5.1.4. Purpurin (**5**).* Yellow powder; ^{1}H NMR (400 MHz, DMSO-d_6): δ H 6.60, brs (H-2), 7.28, brs (H-4), 8.20, brd (H-5&8), 7.67−7.83, m (H-6 &7). ^{13}C NMR (100 MHz, DMSO-d_6): δ C 160.4 (C-1), 104.9 (C-2), 157.0 (C-3), 109.6 (C-4), 126.1 (C-5), 134.8 (C-6), 133.9 (C-7), 126. Three (C-8), 186.4 (C-9), 183.1 (C-10), 133.7 (C-11), 133.2 (C-12), 112.1 (C-13), and 132.3 (C-14).

*2.5.1.5. Nor-damnacanthal (**6**).* Yellow powder; ^{1}H NMR (400 MHz, DMSO-d_6): δ H 7.21, s (H-4), 8.13, dd, J = 8, 2 (H-5), 7.82−7.86, m (H-6&7), 8.07, dd, J = 8, 2 (H- 8), 13.18, s (C1−OH), 9.70, s (COH). ^{13}C NMR (100 MHz, DMSO-d_6): δ C 164.6 (C-1), 117.1 (C-2), 164.1 (C-3), 108.1 (C-4), 127.2 (C-5), 134.9 (C-6), 135.1 (C-7), 126.8 (C-8), 186.7 (C-9), 182.2 (C-10), 134.4 (C-11), 133.4 (C-12), 109.5 (C-13), 133.3 (C-14), 191.4 (COH).

*2.5.1.6. Emodin (**7**).* Orange powder; ^{1}H NMR (600 MHz, $CDCl_3$): δ H 7.08, brs (H-2), 7.62, brs (H-4), 7.28, brs (H-5), 6.67, brs (H-7), 2.45, s (CH_3), 12.11, s (C1−OH), 12.28, s

https://doi.org/10.1021/acsomega.4c09853
ACS Omega 2025, 10, 13027−13045

(C8−OH). ^{13}C NMR (150 MHz, $CDCl_3$): δ C 162.5 (C-1), 124.6 (C-2), 148.4 (C-3), 121.3 (C-4), 108.8 (C-5), 165.2 (C-6), 108.9 (C-7), 163.4 (C-8), 190.8 (C-9), 182.0 (C-10), 133.1 (C-11), 110.4 (C-12), 113.6 (C-13), 135.3 (C-14), 22.7 (CH_3).

As previously mentioned in the experimental section, eight compounds were isolated and purified (Figure 6). Compounds **1** and **8** were identified through comparison with reference authentic samples as scopoletin and rutin, respectively. Compounds **2**−**7** were identified based on NMR data as well as comparison with the previously published data. Compound **2** was identified as rubiadin,[79] compound **3**, chrysophanic acid;[80] compound **4**, alizarin;[81] compound **5**, purpurin;[82] compound **6**, nor-damnacanthal;[83] and finally compound **7** was identified as emodin[84] (Figure 6).

2.6. Quantitation of Alizarin and Purpurin Using LC/MS Analysis. The method was optimized as illustrated in Table S5. Validation of the method was verified as follows:

2.6.1. Linearity. Evaluation of the linearity of the method was performed by analyzing a number of different concentrations of each alizarin and purpurin as standard solutions. Each concentration was applied in triplicate, and their data of the calibration curve showed a good linear relationship over the concentration range of 50−200 ng/mL for alizarin and 25−250 ng/mL for purpurin. The correlation coefficient (R^2) was 0.9925 for alizarin and 0.9986 for purpurin. The linear regression equations were found to be $y = 2.226x + 57.167$ and $y = 1.4771x + 181$ for alizarin and purpurin, respectively, where y is the peak area, and x is the concentration of analyte.

2.6.2. System Precision. The system precision was checked by the determination of a selected concentration (100 ng/mL) of the two standard compounds each in triplicate. The value of percent relative standard deviation (%RSD) was found to be 0.86 and 0.95 for alizarin and purpurin, respectively, indicating precision of the method.

2.6.3. Method Precision. This was confirmed by the repeated analysis of the *R. tinctorum* root extract. It was applied 4 times using the same previously described procedure. The low value of %RSD (2.74 and 1.88 for alizarin and purpurin, respectively) indicated the precision of the method.

2.6.4. Accuracy. The accuracy of the suggested method was indicated by the addition of the preanalyzed *R. tinctorum* root extract to a known concentration of standard alizarin, and then, the same sample was fortified by the addition of a known concentration of standard purpurin. The fortified samples were analyzed using the same previously described method. After triplicate analysis of the mixtures. The calculated percentage recovery indicated the accuracy of the procedure.

2.6.5. Limits of Detection and Quantification. The limits of detection and quantification were calculated using the equations 3.3 (SDy/S) for determining the limit of detection and 10 (SDy/S) for the limit of quantification, where SDy is the standard deviation of the response, and S is the slope of the calibration curve.

2.6.6. Sample Analysis. After application of the mentioned method, the concentrations of the two compounds alizarin and purpurin were calculated and found to be 5.2 and 1.8 mg/g of *R. tinctorum* root extract, respectively (Figure S4).

2.7. Identification of the Semisynthetic Derivatives of Alizarin (A1−A3). Chemical modification of the bioactive components of medicinal herbs is one of the most common approaches used in drug discovery. The α- and β-OH groups of alizarin had different reactivity because of the formation of an intramolecular H-bonding between the α-OH and the anthraquinone carbonyl (Figure 7). Differences in the acidity and the ability of bases to deprotonate them were used to synthesize different derivatives.[85]

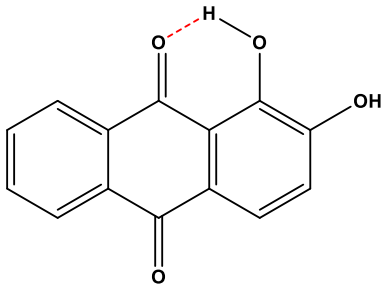

Figure 7. Intramolecular H-bonding in the alizarin molecule.

The synthetic steps for the preparation of alizarin's semisynthetic derivatives are shown in the scheme presented in Figure 8. The prepared derivatives can be divided into two groups: acetyl derivatives and a methyl one. An equimolar ratio of reactants (dimethyl sulfate and acetic anhydride) were the best conditions for synthesizing the monosubstituted derivatives. Poly substituted derivatives were produced if an excess of reagent was used.

The purity of the prepared derivatives was checked by TLC, and their identities were confirmed by ^{1}H NMR data:

2.7.1. 1-Hydroxy-2-methoxyanthracene-9,10-dione or 2-Methyl Alizarin (A1). ^{1}H NMR (400 MHz, DMSO-d_6) δ: 12.67 (s, 1H), 8.28−8.20 (m, 2H), 7.97−7.94 (m, 2H), 7.79 (d, J = 8.5 Hz, 1H), 7.48 (d, J = 8.5 Hz, 1H), 3.96 (s, 3H).[86]

2.7.2. 9,10-Dihydro-1-hydroxy-9,10-dioxoanthracen-2-yl Acetate or Alizarin-2-acetate (A2). ^{1}H NMR (400 MHz, DMSO-d_6) δ: 12.53 (s, 1H), 8.18−8.06 (m, 2H), 7.98−7.87 (m, 3H), 7.42 (d, J = 8.3 Hz, 1H), 2.37 (s, 3H).[87]

2.7.3. 1,2-Diacetoxyanthraquinone or Alizarin-1,2-diacetate (A3). ^{1}H NMR (400 MHz, DMSO-d_6) δ: 8.24−8.22 (m, 1H), 8.19−8.12 (m, 2H), 7.93−7.90 (m, 2H), 7.86 (d, J = 8 Hz, 1H), 2.44 (s, 3H), 2.38 (s, 3H).[88]

The chemical shift near 3.96 ppm is assigned to the three hydrogen atoms in the methoxy group in compound **A1**. However, the chemical shift near 2.37 ppm is assigned to the three hydrogen atoms in the ester side chain in compound **A2**. On the other hand, chemical shifts near 2.38 and 2.44 ppm are assigned to the six hydrogen atoms in the two ester side chains. This demonstrates that the acetylation product is exactly the diacetylated alizarin **A3**.

2.8. In Vitro Cytotoxic Activity Testing of *R. tinctorum* Crude Extracts, Alizarin, Purpurin, and Alizarin Derivatives Using the MTT Assay. Evidence of the anticancer activities of *R. tinctorum* against various types of malignancies has been acquired in numerous biological investigations.[19,20,89] These antitumor activities are mediated by different mechanisms such as inhibition of the proliferation, adhesion and migration of melanoma cells, and targeting multiple signal transduction pathways, modulate cancer aneuploidy, tubulin binding, topoisomerases, and gene-specific targets.[19,20] Hence, purpurin, alizarin, alizarin derivatives, the crude chloroform, hexane, and ethyl acetate extracts of *R. tinctorum* were screened for their cytotoxic activities against a panel of cancerous breast, liver, and noncancerous cell lines, MCF-7, MDA-MB-231, HepG2, and HSF, and to test their safety (selectivity) using the MTT assay (Table 5). Doxorubicin was adopted as a positive

https://doi.org/10.1021/acsomega.4c09853
ACS Omega 2025, 10, 13027−13045

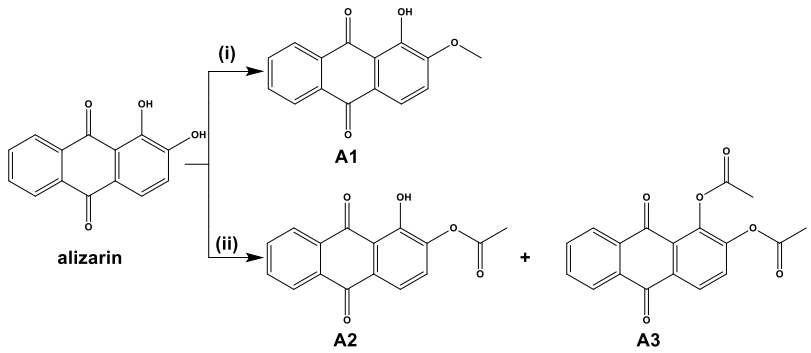

Figure 8. Scheme for the synthesis of alizarin derivatives.

Table 5. In Vitro Cytotoxic Activity Testing of *R. tinctorum* Crude Extracts, Alizarin, Purpurin, and Alizarin Derivatives Using the MTT Assay[a]

sample	IC_{50} (μg/mL)			
	MCF-7*	MDA-MB-231*	HepG2*	HSF*
crude extract	60.58	114.7	88.13	79.23
chloroform extract (RC)	3.987	37.9	22.26	15.49
ethyl acetate extract (RE)	25.74	76.25	85.52	68
hexane extract (RH)	112.1	119.9	142.1	110.1
alizarin-1,2-diacetate (F3−2)	135	126.9	≥50	141.8
alizarin-2-acetate (F3−1)	119.5	156.7	≥50	150.8
2-methyl alizarin (Me)	52.09	83.02	8.878	67.03
alizarin (AZ)	66.9	52.6	99.39	111
purpurin (Pr)	147.9	244.3	179.4	200.7

[a]MCF-7* and MDA-MB-231*: breast cancer; HepG2*: liver cancer; HSF*: normal cell line.

control with depicted IC_{50} = 2.48 μg/mL, 7.05 μg/mL, and 2.17 μg/mL at HepG2, MDA-MB-231, and MCF-7 cell lines, respectively. The chloroform extract of *R. tinctorum* was most cytotoxic against the MCF-7 cell line (IC_{50} = 3.987 μg/mL) with cell growth inhibition of 17.4% at the highest concentration 200 μg/mL (Figure 9C), while it was selective against the MDA-MB-231 with a higher IC_{50} value of 37.9 μg/mL (Figure 9B). Also, the ethyl acetate extract of *R. tinctorum* is cytotoxic against the MCF-7 line (IC_{50} = 25.74 μg/mL) (Figure 9C) and safe against HSF normal cells (Figure 9A).

2-Methyl alizarin (alizarin derivative) was the most cytotoxic against the **HepG2** cell line (IC_{50} = 8.878 μg/mL) (Figure 9D) and safe against HSF normal cells (Figure 9A).

We acknowledge that cytotoxicity data (IC_{50}) of the plant extracts and only 2-methyl alizarin were at the two-digit micrograms per milliliter concentrations for the normal cell line (HSF), which is considerably high as compared to their corresponding data on some cancerous cell lines. Hence, both on-and off-target affinity should be further improved in future studies. Together with the insights from the in silico data structures presented here, both the synthesized compounds (A1−3) offer promising starting points for such future investigations.

2.8.1. RC. Chloroform extract, RE: ethyl acetate extract, RH: hexane extract, F3−2: alizarin-1,2-diacetate, F3−1: alizarin-2-acetate, Me: 2-methyl alizarin, AZ: alizarin, and Pr: purpurin.

3. MATERIALS AND METHODS

3.1. Assembling of *R. tinctorum* In-House Database. A database of *R. tinctorum* was gathered through searching previous literature on *R. tinctorum* chemical makeup (Table S1).[9,12,30−33] The database compounds' 2D structures were verified via ChEMBL (https://www.ebi.ac.uk/chembl/) and PubChem (https://pubchem.ncbi.nlm.nih.gov/). Thereafter, these structures were transformed into the SMILES format by means of Schrodinger software (2017A).

3.2. ADME and Drug-likeness Screening of *R. tinctorum* Database. *R. tinctorum* database metabolites were screened for their drug-likeness by calculating their absorption, distribution, metabolism, and excretion (ADME) properties and pursuing the rule of five of Lipinski,[34] by means of Qikprop software (Schrodinger suite 2017A). Compounds with a calculated OB of lower than 30 were not included in this investigation. Furthermore, compounds that met fewer than three of Lipinski's rule of five criteria were also eliminated.

3.3. Network Pharmacology Analysis. *3.3.1. Identification of Cancer-Related Proteins for R. tinctorum Filtered Metabolites.* Recognition of target proteins associated with the filtered *R. tinctorum* constituents was fulfilled through STITCH DB (http://stitch.embl.de/, ver. 5.0) with the '*H. sapiens*' species setting.[90] UniProt (http://www.uniprot.org/) and GeneCards: the human gene database (http://www.genecards.org/) was searched for information about the recognized genes such as genes ID, names, organism, and role.[90,91] The only genes that remained in the study are the '*H. sapiens*' genes that are linked to cancer. The interactions among the selected genes were visualized through STRING database (https://string-db.org/) that constructed the protein−protein interaction network (PPI network).[27]

3.3.2. Gene Ontology Enrichment Analysis of the Selected Genes. The KEGG pathways (http://www.genome.jp/kegg/pathway.html) and the database for Annotation, Visualization, and Integrated Discovery (DAVID) ver. 6.8 (https://david.ncifcrf.gov/) were looked for data about GO and characterize the canonical pathways, molecular functions, cellular components, and biological processes that are in association with the recognized target genes.[24,27,28] The only picked out pathways are those with adjusted *P*-values ≤0.01 (*P*-values were corrected using the Benjamini−Hochberg method[54] to minimize false positives).

3.3.3. Constructing the Networks. Three networks (constituent-gene, gene-pathway, and constituent-gene-pathway networks) were instituted utilizing Cytoscape 3.8.2 (http://

https://doi.org/10.1021/acsomega.4c09853
ACS Omega 2025, 10, 13027−13045

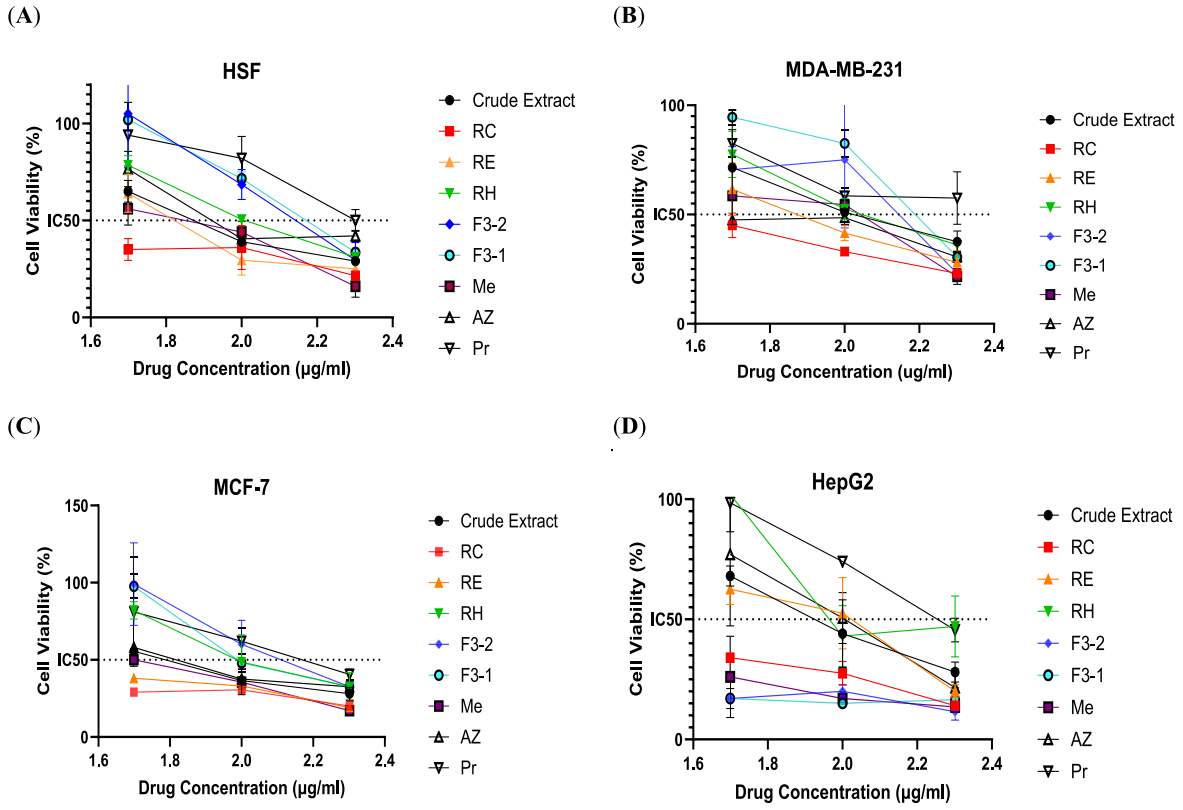

Figure 9. In vitro cytotoxic activity of *R. tinctorum* crude extracts, alizarin, purpurin, and alizarin derivatives using the MTT assay on normal cell line, HSF (A), breast cancer cell lines, MDA-MB-231 (B) and MCF-7 (C), and liver cancer cell line, HepG2 (D).

www.cytoscape.org/) for exploring the multilevel mechanisms underlying *R. tinctorum* constituents' anticancer activity.[29] Genes, constituents, and pathways are represented by the nodes in these networks, and the interactions among them are denoted by the edges. The Cytoscape's network analyzer plug-in was hired to compute the constructed networks' parameters where the importance of the networks' nodes was estimated by the Cytoscape combined score of interactions.

3.4. Molecular Docking Studies. The PDB[92] (https://www.rcsb.org/) was hired to get the three crystal structures of each of the identified most enriched cancer-related targets disclosed from network pharmacology analysis, which were 1-phosphatidylinositol 4,5-bisphosphate phosphodiesterase gamma-1 (PLCG1), apoptosis regulator Bcl-2 (BCL2), cytochrome P450 1B1 (CYP1B1), histone-lysine *N*-methyltransferase NSD2 (NSD2), and estrogen receptor beta (ESR2). The crystal structures were selected to have a high resolution, with their source organism being *Homo sapiens*. The three crystal structures of each protein were compared using the two procedures: the first is the redocking procedure, in which the cocrystallized ligands were docked back into the receptor binding cavity. The root-mean-square deviation (RMSD) value between the initial conformation and the redocked one was calculated for each crystal structure.[62,63] The second procedure is the enrichment calculations, in which a validation set comprising active compounds for each of the investigated proteins was seeded into 1000 built-in Schrodinger decoys (Table S3). Decoys are compounds that are similar in physical properties with respect to the reference ligand that might not bind effectively to a protein. Validation parameters such as receiver operating characteristic (ROC), AUC-ROC, BED-ROC, and enrichment factor (EF at 2%, 5%, and 10%) were then estimated.[62,63] The crystal structure displaying the lowest RMSD and best enrichment values for each protein was chosen for further docking with *R. tinctorum*'s hit anticancer phytoconstituents.

The crystal structures were saved in the form of pdb files to be subsequently prepared through the PrepWiz module incorporated into the Schrodinger software.[93] The first step was protein preprocessing by specifying hydrogens and bond orders and formation of disulfide bonds and zero order bonds with metals. Every water molecule that had >5 Å was eliminated from the active site. Hydrogen bonds' assignment was carried out through PROPKA. Afterward, energy was reduced via OPLS 3 force field until the reduced structure's RMSD was above 0.30 Å when compared with the crystal structure.[94] By applying the receptor grid creation module, the binding site's location was determined for the docking studies, and the grids were the boxes that include the cocrystallized ligands' centroids.

To gain low-energy compounds' structures, their 3D structures were uploaded in SDF format into the LigPrep module built in the Maestro molecular modeling platform. Ionization state regulation was done to generate every probable state at pH 7. Simulation of the docking experiments was accomplished by means of the extra-precision (XP-Glide) module of the Glide docking program incorporated into the Maestro molecular modeling platform. The Maestro interface was hired to visualize the ligand−target interactions, encompassing hydrogen bonds, ion pair, and hydrophobic interactions, in addition to the binding modes of the ligands.

3.5. Plant Material. The source of *R. tinctorum* roots was the Egyptian market, and confirmation of the identity was done at Suez Canal University (Faculty of Science). A voucher specimen was held over at the Faculty of Pharmacy (Pharmacognosy

https://doi.org/10.1021/acsomega.4c09853
ACS Omega 2025, 10, 13027−13045

Department), Suez Canal University. The sample was given a code number 2019-RT.

3.6. Isolation of Some of the Hit Anticancer Metabolites from the Roots of *R. tinctorum*. Column chromatographic separations of the pure compounds were possible by using Sephadex LH-20 (0.25−0.1 mm, Pharmacia) as well as silica gel 60 (0.04−0.063 mm). Thin layer chromatographic separation was done using TLC plates and precoated with silica gel 60 F254 (0.2 mm, Merck). The solvents utilized for extraction and development such as chloroform and methanol were purchased from Merck Company (Darmstadt, Germany). Visualization of the spots was carried out by UV absorption (λ_{max} 255 and 366 nm) and exposure to conc. ammonia vapor, while the purity was inspected by a *P*-anisaldehyde/H_2SO_4 spray.

Roots were dried and powdered, where 2 kg of the powder was extracted by methanol then dried using rotary evaporator to give finally 250 g of dry brownish-red residue. The dry extract (160 g were used) was suspended in 150 mL of distilled water. This step was followed by successive fractionation with hexane, chloroform, and ethyl acetate (3 L of each). After drying of the extracts, the obtained yield was found to be 28, 65, and 42 g of hexane, chloroform, and ethyl acetate extracts, respectively. The chloroform extract showed the most major and distinct spots, as well as positive results when tested for the presence of anthraquinones and showed the best cytotoxic activity. Therefore, the sample was subjected to further fractionation. A weight of 18 mg of the chloroform extract was applied on a column packed with silica gel and fractionated using $CHCl_3$/MeOH gradient elution to yield 6 main fractions (after compiling of similar fractions together). These fractions were subjected to different chromatographic techniques including adsorption (column and thin layer chromatography) and size exclusion using Sephadex to give finally 8 pure compounds.

NMR data were obtained using Bruker Avance DRX 600 MHz spectrometers, while chemical shifts were recorded in parts per million and coupling constants in Hz, and $CDCl_3$ and CD_3OD were used as solvents.

3.7. Quantitation of Alizarin and Purpurin Using LC/MS Analysis. An amount of 50 mg of each of alizarin and purpurin was used to prepare the standard stock solution. The prepared solutions were quantitatively placed in a 10 mL volumetric flask, and methanol was used to adjust the volume. The stock solution was tightly closed and kept in a refrigerator until used for preparing different concentrations in order to construct the calibration curve. Different concentrations of each of alizarin and purpurin were prepared, and optimization of mass spectrometric parameters for the LC−MS analysis was performed. For LC−MS analysis, a Waters ACQUITY Xevo TQD UPLC/MS system was used. The data acquisition was implemented using MassLynx version V4.1 SCN918 software. Samples and standard solutions were separated on an ACQUITY UPLC HSS T3 C18, 1.8 μm, 50 mm × 2.1 mm column at 30 °C. Chromatographic separations were executed using gradient elution by 0.1% (v/v) formic acid in water (eluent A) and 0.1% (v/v) formic acid in acetonitrile (eluent B) with a rate of flow equal to 0.3 mL/min. Analytes were detected with electrospray ionization (ESI) in positive mode for alizarin and negative mode for purpurin, and the injected volume was 10 μL. The drying gas was operated at a flow rate of 650 L h^{-1} at 350 °C, the cone gas flow was 20 L h^{-1}, the cone voltage was 40 V, and the capillary was set at 3000 V.

3.8. Preparation and Purification of the Semisynthetic Derivatives of Alizarin (A1−A3). *3.8.1. Chemicals and Reagents.* Acetic anhydride, dimethyl sulfate, potassium carbonate, pyridine, and solvents used in the preparation of the semisynthetic derivatives were purchased from Sigma-Aldrich (St. Louis, Mo., USA).

3.8.2. Experimental Section. 3.8.2.1. Procedure for Methylation. A solution of alizarin (0.2 mmol) and potassium carbonate (42 mg, 0.3 mmol) together with dimethyl sulfate (0.02 mL, 0.2 mmol) in the presence of acetone (5 mL) was refluxed for 5 h. Removal of acetone was performed under vacuum followed by washing of the resulting mixture with 5 mL of water. Ethyl acetate (3 × 5 mL) was used for extraction of the aqueous layer, then the solvent was eliminated under vacuum, and purification of the obtained residue was done by preparative thin layer chromatography with ethyl acetate−hexane (30:70) as the eluent to give pure compound (A1).[95]

3.8.2.2. Procedure for Acetylation. Acetic anhydride (0.02 mol) was added to a solution of 0.2 mmol of alizarin in 2 mL of pyridine. Vigorous stirring of the solution was done overnight, and then the solvent was removed. The resulting concentrated solution was worked up with H_2O, acidified by HCl, extracted with ethyl acetate, and dried over Na_2SO_4, filtered, and concentrated. The products were purified using preparative thin layer chromatography, while the used eluent was a mixture of ethyl acetate and hexane in a ratio of 30:70 to give pure compound (A2).[87,88] Performing the reaction with a 2-fold excess gave compound (A3).[88]

3.9. In Vitro Cytotoxic Activity Testing of *R. tinctorum* Crude Extracts, Alizarin, Purpurin, and Alizarin Derivatives. *3.9.1. Cell Culture Treatment.* *R. tinctorum* crude extracts, alizarin, purpurin, and alizarin derivatives were tested using cancerous breast, liver, as well as noncancerous cell lines, MCF-7, MDA-MB-231, HepG2, and HSF, that were kept in RPMI-1640/DMEM (purchased from Sigma-Aldrich, St. Louis, MO, USA). The media were complemented with 2 mML-glutamine, 1% penicillin/streptomycin (Lonza, Belgium), and 10% FBS (Sigma, St. Louis, MO, USA). All cells were incubated in 5% CO_2 atmosphere (NuAire, Lane Plymouth, MN 55447, USA) at 37 °C as reported in the routine tissue culture method.[96]

3.9.2. Cytotoxicity Using the MTT Assay. A 96-well plate was used where the cells were plated in triplicate at a density of 5000 cells. Treatment of the cells was executed on the next day using the indicated extract and compound/s at the specified concentrations, while the final volume of the media was 100 μL. Viability of the cells was counted after 48 h using MTT solution (Promega, Madison, WI, USA).[97] Twenty μL of the reagent was added to each well, then the plate was incubated for 3 h, and fluorescence was determined (570 nm) by a plate reader. Finally, IC_{50} values were estimated using GraphPad prism 7.[98,99]

4. CONCLUSIONS

The application of network pharmacology with molecular docking for the first time in this study enabled us to disclose the hit anticancer *R. tinctorum* constituents. Additionally, the identification of PLCG1, BCL2, CYP1B1, NSD2, and ESR2 as the most enriched cancer-linked target genes was allowed. Moreover, acacetin and alizarin were declared to possess the lowest binding energy on the active sites of NSD2 and BCL2, respectively, while anthragallol showed the most stabilized interactions on the active sites of PLCG1, CYP1B1, and ESR2. The anticipated anticancer efficacy of crude *R. tinctorum* root extracts, some isolated metabolites, and semisynthetic deriva-

https://doi.org/10.1021/acsomega.4c09853
ACS Omega 2025, 10, 13027−13045

tives was assured by evaluating their in vitro cytotoxic potentials on normal, breast, and liver cancer cell lines. The remarkable results were shown by *R. tinctorum* chloroform extract, which demonstrated the most cytotoxic activity against the MCF-7 cell line, whereas 2-methyl alizarin was the most cytotoxic against the HepG2 cell line. Given the current limitation regarding the safety profile, future studies will be directed toward gaining better selectivity indices for the plant-derived metabolites. A basis for such investigations will be the structure-guided approaches and computational investigation established in this study. Further in vivo and clinical studies are required for these extracts and metabolites to prove their bioavailability and stability and also to assess the possibility of being formulated into effective marketed anticancer agents.

■ ASSOCIATED CONTENT

Data Availability Statement

The data supporting this article have been included as part of the Supporting Information.

Supporting Information

The Supporting Information is available free of charge at https://pubs.acs.org/doi/10.1021/acsomega.4c09853.

Database of the chemical constituents of *R. tinctorum*; synopsis of PubMed search results on top hit *R. tinctorum* constituents in cancer management; structural features of active compounds used in enrichment studies for each of the investigated target protein; validation parameters for molecular docking of three crystal structures for each studied protein; validation parameters of the method for the estimation of alizarin and purpurin; network of compound−target gene interactions for *R. tinctorum* constituents by linking 22 compounds and 32 cancer-related target proteins; protein−protein interaction (PPI) network of identified cancer-related targets; gene−pathway network (genes are presented in blue color, and pathways are presented in green color); and MS chromatogram for the injection of the standard 100 ng alizarin, 50 ng purpurin, and the samples (PDF)

■ AUTHOR INFORMATION

Corresponding Authors

Jihan M. Badr − *Department of Pharmacognosy, Faculty of Pharmacy, Suez Canal University, Ismailia 41522, Egypt*; Email: gehan_ibrahim@pharm.suez.edu.eg

Reda F. A. Abdelhameed − *Department of Pharmacognosy, Faculty of Pharmacy, Suez Canal University, Ismailia 41522, Egypt; Department of Pharmacognosy, Faculty of Pharmacy, Galala University, New Galala 43713, Egypt*; Email: reda.fouad@gu.edu.eg

Authors

Alaa A. El-Banna − *Department of Pharmacognosy, Faculty of Pharmacy, Alexandria University, Alexandria 21521, Egypt; Department of Pharmacognosy, College of Pharmacy, Najran University, Najran 66454, Saudi Arabia*

Enas E. Eltamany − *Department of Pharmacognosy, Faculty of Pharmacy, Suez Canal University, Ismailia 41522, Egypt*

Asmaa S. A. Yassen − *Department of Medicinal Chemistry, Faculty of Pharmacy, Galala University, New Galala 43713, Egypt; Department of Pharmaceutical Organic Chemistry, Faculty of Pharmacy, Suez Canal University, Ismailia 41522, Egypt*; orcid.org/0000-0002-7956-9739

Ahmed Lotfy − *Egyptian Liver Research Institute and Hospital (ELRIAH), Mansoura 35111, Egypt; Department of Surgery, Medical University of South Carolina, Charleston, South Carolina 29425, United States*

Aya H. H. El-Tanahy − *Department of Pharmacognosy, Faculty of Pharmacy, Delta University for Science and Technology, Gamasa 7730103, Egypt*

Mardi M. Algandaby − *Department of Biological Sciences, Faculty of Science, King Abdulaziz University, Jeddah 21589, Saudi Arabia*

Samar S. Murshid − *Department of Natural Products and Alternative Medicine, Faculty of Pharmacy, King Abdulaziz University, Jeddah 21589, Saudi Arabia*; orcid.org/0000-0002-9370-4546

Sameh S. Elhady − *Department of Biological Sciences, Faculty of Science, King Abdulaziz University, Jeddah 21589, Saudi Arabia*; orcid.org/0000-0003-3799-0581

Complete contact information is available at: https://pubs.acs.org/10.1021/acsomega.4c09853

Author Contributions

‡‡A.A.E.-B. and E.E.E. contributed equally to this manuscript and are co-first authors. A.A.E-B.: data curation, formal analysis, writing—original draft; E.E.E.: conceptualization, methodology, investigation, formal analysis, writing—original draft; A.S.A.Y.: conceptualization, methodology, investigation, writing—original draft; A.L.: conceptualization, investigation, writing—original draft; A.H.H.E-T.: conceptualization methodology, investigation, writing—original draft; J.M.B.: conceptualization, methodology, investigation, formal analysis, writing—review and editing; M.M.A.: investigation, data curation, writing—original draft, writing—review and editing; S.S.M.: investigation, writing—original draft, data curation, writing—review and editing; S.S.E.: conceptualization, methodology, investigation, formal analysis, writing—review and editing; and R.F.A.A.: conceptualization, methodology, writing—review and editing.

Notes

The authors declare no competing financial interest.

■ ACKNOWLEDGMENTS

This project was funded by the Deanship of Scientific Research (DSR) at King Abdulaziz University (KAU), Jeddah, Saudi Arabia, under grant number: (GPIP-1933-130-2024). The authors, therefore, acknowledge with thanks DSR for technical and financial support. The simulations in this work were performed at King Abdulaziz University's High Performance Computing Center (Aziz Supercomputer) (http://hpc.kau.edu.sa)", and the authors, therefore, acknowledge with thanks the center for technical support. The authors would like to thank Associate Professor Khaled M. Darwish, Department of Medicinal Chemistry, Faculty of Pharmacy, Galala University, New Galala, Egypt, for his guidance support to finalize this work.

■ REFERENCES

(1) Hassanpour, S. H.; Dehghani, M. Review of Cancer from Perspective of Molecular. *J. Cancer Res. Pract.* **2017**, *4*, 127−129.

(2) Nagai, H.; Kim, Y. H. Cancer Prevention from the Perspective of Global Cancer Burden Patterns. *J. Thorac. Dis.* **2017**, *9*, 448−451.

(3) Siegel, R. L.; Miller, K. D.; Sandeep, N.; Mbbs, W.; Ahmedin, I.; Dvm, J.; Siegel, R. L. Cancer Statistics, 2023. *CA Cancer J. Clin.* **2023**, *73* (1), 17−48.

(4) Debela, D. T.; Muzazu, S. G. Y.; Heraro, K. D.; Ndalama, M. T.; Mesele, B. W.; Haile, D. C.; Kitui, S. K.; Manyazewal, T. *New*

Approaches and Procedures for Cancer Treatment: Current Perspectives; SAGE Open Medicine. SAGE Publications Ltd, 2021.
(5) Feron, O.; Abalo, R.; Nurgali, K.; Jagoe, R. T. Editorial: Adverse Effects of Cancer Chemotherapy: Anything New to Improve Tolerance and Reduce Sequelae? Editorial on the Research Topic Adverse Effects of Cancer Chemotherapy: Anything New to Improve Tolerance and Reduce Sequelae? *Front. Pharmacol.* **2018**, *1*, 245.
(6) Desai, A. G.; Qazi, G. N.; Ganju, R. K.; El-Tamer, M.; Singh, J.; Saxena, A. K.; Bedi, Y. S.; Taneja, S. C.; Bhat, H. K. Medicinal Plants and Cancer Chemoprevention. *Curr. Drug Metab.* **2008**, *9* (7), 581−591.
(7) Kooti, W.; Servatyari, K.; Behzadifar, M.; Asadi-Samani, M.; Sadeghi, F.; Nouri, B.; Zare Marzouni, H. Effective Medicinal Plant in Cancer Treatment, Part 2: Review Study. *J. Evidence-Based Complementary Altern. Med.* **2017**, *22*, 982−995.
(8) Ibrahim, R. S.; El-Banna, A. A. Royal Jelly Fatty Acids Bioprofiling Using TLC-MS and Digital Image Analysis Coupled with Chemometrics and Non-Parametric Regression for Discovering Efficient Biomarkers against Melanoma. *RSC Adv.* **2021**, *11* (31), 18717−18728.
(9) Nejad, H. E.; Nejad, A. E. Rubia Tinctorum L. (Rubiaceae) or Madder as One of the Living Color to Dyeing Wool, 2013; Vol. *1*. http://www.ijabbr.com.
(10) Ozdemir, M. B.; Karadag, R. M.; Rubia, T. L. Madder (*Rubia tinctorum* L.) as an Economic Factor Under Sustainability Goals in the Textile Dyeing. *J. Nat. Fibers* **2023**, *20* (1), 2128968.
(11) Shilpa, P. N.; Venkatabalasubramanian, S.; Devaraj, S. N. Ameliorative Effect of Methanol Extract of Rubia Cordifolia in N-Nitrosodiethylamine-Induced Hepatocellular Carcinoma. *Pharm. Biol.* **2012**, *50* (3), 376−383.
(12) Derksen, G. C. H.; Van Beek, T. A.; Rubia Tinctorum, L.; ur-Rahman, A. *Studies in Natural Products Chemistry*, 26 ed.; Elsevier Science B.V., 2002; pp 629−684.
(13) Ghandehari, S.; Tabrizi, M. H.; Ardalan, P.; Neamati, A.; Shali, R. Green Synthesis of Silver Nanoparticles Using Rubia Tinctorum Extract and Evaluation the Anti-Cancer Properties in Vitro. *IET Nanobiotechnol.* **2019**, *13* (3), 269−274.
(14) Marhoume, F. Z.; Aboufatima, R.; Zaid, Y.; Limami, Y.; Duval, R. E.; Laadraoui, J.; Belbachir, A.; Chait, A.; Bagri, A. Antioxidant and Polyphenol-Rich Ethanolic Extract of Rubia Tinctorum L. Prevents Urolithiasis in an Ethylene Glycol Experimental Model in Rats. *Molecules* **2021**, *26* (4), 1005.
(15) Sharifzadeh, M.; Ebadi, N.; Manayi, A.; Kamalinejad, M.; Rezaeizadeh, H.; Mirabzadeh, M.; Yazdi, B. B.; Khanavi, M. Effect of Rubia Tinctorum L. Extractson Carrageenan-Induced Paw Edema in Rats. *J. Med. Plants* **2014**, *13* (51), 62−70.
(16) Manojlovic, N. T.; Solujic, S.; Sukdolak, S.; Milosev, M. Antifungal Activity of Rubia Tinctorum, Rhamnus Frangula and Caloplaca Cerina. *Fitoterapia* **2005**, *76* (2), 244−246.
(17) Ghafari, R.; Mouslemanie, N.; Nayal, R. Antibacterial Activity of Rubia Tinctorum L. Root Extracts. *Int. J. Pharma Sci. Res.* **2018**, *9* (9), 3914.
(18) Marhoume, F.; Zaid, Y.; Boufous, H.; Errafiy, N.; Laaradia, M.; Laadraoui, J.; Hakmaoui, A.; Bagri, A.; Chait, A. Hepatoprotective Activity of Rubia Tinctorum's Extract against CCl4 Induced Hepatic Injury in Rats. *European J. Med. Plants* **2017**, *20* (4), 1−10.
(19) Lajkó, E.; Bányai, P.; Zámbó, Z.; Kursinszki, L.; Szoke, É.; Kohidai, L. Targeted Tumor Therapy by Rubia Tinctorum L.: Analytical Characterization of Hydroxyanthraquinones and Investigation of Their Selective Cytotoxic, Adhesion and Migration Modulator Effects on Melanoma Cell Lines (A2058 and HT168-M1). *Cancer Cell Int.* **2015**, *15* (1), 119.
(20) Rashan, L.; Hakkim, F. L.; Fiebig, H. H.; Kelter, G.; Merfort, I.; Al-Buloshi, M.; A A Hasson, S. S. In Vitro Anti-Proliferative Activity of the Rubia Tinctorum and Alkanna Tinctoria Root Extracts in Panel of Human Tumor Cell Lines Hasson. *Jordan J. Biol. Sci.* **2018**, *11*, 489. http://researchonline.ljmu.ac.uk/
(21) Abdul Jalill, R. D. H. Phytochemical Analysis of Ficus arnottiana (Miq.) Miq. Leaf Extract Using GC-MS Analysis. *International Journal of Pharmacognosy and Phytochemical Research*; Dr. Yashwant Research Labs Pvt. Ltd., 2017; Vol. *9*(6), pp 286−292.
(22) Rumie Vittar, N. B.; Comini, L.; Fernadez, I. M.; Agostini, E.; Nuñez-Montoya, S.; Cabrera, J. L.; Rivarola, V. A. Photochemotherapy Using Natural Anthraquinones: Rubiadin and Soranjidiol Sensitize Human Cancer Cell to Die by Apoptosis. *Photodiagnosis Photodyn. Ther.* **2014**, *11* (2), 182−192.
(23) Caesar, L. K.; Cech, N. B. Synergy and Antagonism in Natural Product Extracts: When 1 + 1 Does Not Equal 2. In *Natural Product Reports*; Royal Society of Chemistry, 2019; pp 869−888..
(24) Shawky, E.; Nada, A. A.; Ibrahim, R. S. Potential Role of Medicinal Plants and Their Constituents in the Mitigation of SARS-CoV-2: Identifying Related Therapeutic Targets Using Network Pharmacology and Molecular Docking Analyses. *RSC Adv.* **2020**, *10* (47), 27961−27983.
(25) Hong, M.; Zhang, Y.; Li, S.; Tan, H. Y.; Wang, N.; Mu, S.; Hao, X.; Feng, Y. A Network Pharmacology-Based Study on the Hepatoprotective Effect of Fructus Schisandrae. *Molecules* **2017**, *22* (10), 1617.
(26) Chandran, U.; Patwardhan, B. Network Ethnopharmacological Evaluation of the Immunomodulatory Activity of Withania Somnifera. *J. Ethnopharmacol.* **2017**, *197*, 250−256.
(27) El-Banna, A. A.; Darwish, R. S.; Ghareeb, D. A.; Yassin, A. M.; Abdulmalek, S. A.; Dawood, H. M. Metabolic Profiling of Lantana Camara L. Using UPLC-MS/MS and Revealing Its Inflammation-Related Targets Using Network Pharmacology-Based and Molecular Docking Analyses. *Sci. Rep.* **2022**, *12* (1), 14828.
(28) Ibrahim, R. S.; El-Banna, A. A. Network Pharmacology-Based Analysis for Unraveling Potential Cancer-Related Molecular Targets of Egyptian Propolis Phytoconstituents Accompanied with Molecular Docking Andin Vitrostudies. *RSC Adv.* **2021**, *11* (19), 11610−11626.
(29) El-Banna, A. A. An Integrated Approach of Network Pharmacology and Molecular Docking Analyses for Identification of Lepidium Sativum L. Antidiabetic Molecular Targets. *Records of pharmaceutical and biomedical sciences* **2023**, *7* (2), 111−127.
(30) Kawasaki, Y.; Goda, Y.; Yoshihira, K. The Mutagenic Constituents of Rubia Tinctorum. *Chem. Pharm. Bull.* **1992**, *40* (6), 1504−1509.
(31) Zohra, H. F.; Erenler, R.; Hariri, A. Biological Activities and Chemical Composition of Rubia Tinctorum (L) Root and Aerial Part Extracts Thereof. *Acta Biol. Colomb.* **2022**, *27* (3), 403−404.
(32) Behbudi, G.; Hoseinzadeh, A.; Sadeghipour, Y.; Behbudi, G. Investigation Preliminary Antimicrobial and Anticancer Properties: On Topic Rubia Tinctorum Plant by Using Polydimethylsiloxane (CAR/PDMS). *Advances in Applied NanoBio-Technologies*; Dorma Trading, Est. Publishing Manager, 2020; Vol. *1*(1), pp 5−14.
(33) Eltamany, E. E.; Nafie, M. S.; Khodeer, D. M.; El-Tanahy, A. H. H.; Abdel-Kader, M. S.; Badr, J. M.; Abdelhameed, R. F. A. Rubia Tinctorum Root Extracts: Chemical Profile and Management of Type II Diabetes Mellitus. *RSC Adv.* **2020**, *10* (41), 24159−24168.
(34) Lipinski, C. A. Lead- and Drug-like Compounds: The Rule-of-Five Revolution. *Drug Discov. Today Technol.* **2004**, *1* (4), 337−341.
(35) Yang, X.; Guan, Y.; Yan, B.; Xie, Y.; Zhou, M.; Wu, Y.; Yao, L.; Qiu, X.; Yan, F.; Chen, Y.; Huang, L. Evidence-based Complementary and Alternative Medicine Bioinformatics Approach through Network Pharmacology and Molecular Docking to Determine the Molecular Mechanisms of Erjing Pill in Alzheimer's Disease. *Exp. Ther. Med.* **2021**, *22* (5), 1252.
(36) Guan, L.; Yang, H.; Cai, Y.; Sun, L.; Di, P.; Li, W.; Liu, G.; Tang, Y. ADMET-Score − a Comprehensive Scoring Function for Evaluation of Chemical Drug-Likeness. *Medchemcomm* **2019**, *10* (1), 148.
(37) Kuhn, M.; von Mering, C.; Campillos, M.; Jensen, L. J.; Bork, P. STITCH: Interaction Networks of Chemicals and Proteins. *Nucleic Acids Res.* **2007**, *36* (Database), D684−D688.
(38) Bairoch, A.; Apweiler, R.; Wu, C. H.; Barker, W. C.; Boeckmann, B.; Ferro, S.; Gasteiger, E.; Huang, H.; Lopez, R.; Magrane, M.; Martin, M. J.; Natale, D. A.; O'Donovan, C.; Redaschi, N.; Yeh, L. S. L. The Universal Protein Resource (UniProt). *Nucleic Acids Res.* **2005**, *33* (DatabaseIssue), D154.
(39) GeneCards—Human Genes | Gene Database | Gene Search. 2023, https://www.genecards.org/ (accessed Oct 30, 2023).

https://doi.org/10.1021/acsomega.4c09853
ACS Omega 2025, 10, 13027−13045

(40) Zhang, G.; Li, Z.; Dong, J.; Zhou, W.; Zhang, Z.; Que, Z.; Zhu, X.; Xu, Y.; Cao, N.; Zhao, A. Acacetin Inhibits Invasion, Migration and TGF-B1-Induced EMT of Gastric Cancer Cells through the PI3K/Akt/Snail Pathway. *BMC Complementary Med. Ther.* **2022**, *22* (1), 10−12.
(41) Kandhari, K.; Mishra, J. P. N.; Agarwal, R.; Singh, R. P. Acacetin Induces Sustained ERK1/2 Activation and RIP1-Dependent Necroptotic Death in Breast Cancer Cells. *Toxicol. Appl. Pharmacol.* **2023**, *462*, 116409.
(42) Xu, Z.; Hou, Y.; Zou, C.; Liang, H.; Mu, J.; Jiao, X.; Zhu, Y.; Su, L.; Liu, M.; Chen, X.; Qian, C.; Zhu, X.; Gong, W.; Dong, Q.; Zhang, F. Alizarin a Nature Compound, Inhibits the Growth of Pancreatic Cancer Cells by Abrogating NF-KB Activation. *Int. J. Biol. Sci.* **2022**, *18* (7), 2759−2774.
(43) Fotia, C.; Avnet, S.; Granchi, D.; Baldini, N. The Natural Compound Alizarin as an Osteotropic Drug for the Treatment of Bone Tumors. *J. Orthop. Res.* **2012**, *30* (9), 1486−1492.
(44) Yazgan, B.; Mesci, S.; Bayık, N.; Akşahin, M.; Çiftçi, G. Y.; Yıldırım, T. Explorations of ATP-Binding Cassette Transporters and Apoptosis Signal Pathways of 2-Hydroxyanthraquinone Substituted Cyclotriphosphazenes in MCF-7 and DLD-1 Cell Lines. *Anticancer Agents Med. Chem.* **2022**, *22* (6), 1124−1138.
(45) Shi, Y.; Wang, C. H.; Gong, X. G. Apoptosis-Inducing Effects of Two Anthraquinones from Hedyotis Diffusa WILLD. *Biol. Pharm. Bull.* **2008**, *31* (6), 1075−1078.
(46) Bajpai, V. K.; Alam, M. B.; Quan, K. T.; Choi, H. J.; An, H.; Ju, M. K.; Lee, S. H.; Huh, Y. S.; Han, Y. K.; Na, M. K. Cytotoxic Properties of the Anthraquinone Derivatives Isolated from the Roots of Rubia Philippinensis. *BMC Complementary Altern. Med.* **2018**, *18* (1), 200.
(47) Schnoeder, T. M.; Schwarzer, A.; Jayavelu, A. K.; Hsu, C. J.; Kirkpatrick, J.; Döhner, K.; Perner, F.; Eifert, T.; Huber, N.; Arreba-Tutusaus, P.; Dolnik, A.; Assi, S. A.; Nafria, M.; Jiang, L.; Dai, Y. T.; Chen, Z.; Chen, S. J.; Kellaway, S. G.; Ptasinska, A.; Ng, E. S.; Stanley, E. G.; Elefanty, A. G.; Buschbeck, M.; Bierhoff, H.; Brodt, S.; Matziolis, G.; Fischer, K. D.; Hochhaus, A.; Chen, C. W.; Heidenreich, O.; Mann, M.; Lane, S. W.; Bullinger, L.; Ori, A.; von Eyss, B.; Bonifer, C.; Heidel, F. H. PLCG1 Is Required for AML1-ETO Leukemia Stem Cell Self-Renewal. *Blood* **2022**, *139* (7), 1080.
(48) Thomadaki, H.; Scorilas, A. BCL2 Family of Apoptosis-Related Genes: Functions and Clinical Implications in Cancer. *Crit. Rev. Clin. Lab Sci.* **2006**, *43* (1), 1−67.
(49) Chen, C.; Yang, Y.; Guo, Y.; He, J.; Chen, Z.; Qiu, S.; Zhang, Y.; Ding, H.; Pan, J.; Pan, Y. CYP1B1 Inhibits Ferroptosis and Induces Anti-PD-1 Resistance by Degrading ACSL4 in Colorectal Cancer. *Cell Death Dis.* **2023**, *14* (4), 271.
(50) Zhao, L.; Li, Q.; Huang, Z. J.; Sun, M. X.; Lu, J.; Zhang, X.; Li, G.; Wu, F. Identification of Histone Methyltransferase NSD2 as an Important Oncogenic Gene in Colorectal Cancer. *Cell Death Dis.* **2021**, *12* (11), 974−1010.
(51) Dalal, H.; Dahlgren, M.; Gladchuk, S.; Brueffer, C.; Gruvberger-Saal, S. K.; Saal, L. H. Clinical Associations of ESR2 (Estrogen Receptor Beta) Expression across Thousands of Primary Breast Tumors. *Sci. Rep.* **2022**, *12* (1), 4696.
(52) Kanehisa, M.; Goto, S. KEGG: Kyoto Encyclopedia of Genes and Genomes. *Nucleic Acids Res.* **2000**, *28* (1), 27−30.
(53) Dennis, G.; Sherman, B. T.; Hosack, D. A.; Yang, J.; Gao, W.; Lane, C.; Lempicki, R. A. *DAVID: Database for Annotation, Visualization, and Integrated Discovery*; DAVID, 2003; Vol. *4*, p P3. http://dot.ped.med.umich.edu:2000/.
(54) Ferreira, J. A.; Zwinderman, A. H. On the Benjamini-Hochberg Method. *Ann. Stat.* **2006**, *34* (4), 1827−1849.
(55) Meng, X.-Y.; Zhang, H.-X.; Mezei, M.; Cui, M. Molecular Docking: A Powerful Approach for Structure-Based Drug Discovery. *Curr. Comput. Aided Drug Des.* **2011**, *7* (2), 146.
(56) Samarina, N.; Ssebyatika, G.; Tikla, T.; Waldmann, J. Y.; Abere, B.; Nanna, V.; Marasco, M.; Carlomagno, T.; Krey, T.; Schulz, T. F. Recruitment of Phospholipase Cγ1 to the Nonstructural Membrane Protein PK15 of Kaposi Sarcoma-Associated Herpesvirus Promotes Its Src-Dependent Phosphorylation. *PLoS Pathog.* **2021**, *17* (6), No. e1009635.
(57) Singh, K.; Briggs, J. M. Functional Implications of the Spectrum of BCL2Mutations in Lymphoma. In *Mutation Research—Reviews in Mutation Research*; Elsevier B.V., 2016; pp 1−18..
(58) Panneerselvam, S.; Yesudhas, D.; Durai, P.; Anwar, M. A.; Gosu, V.; Choi, S. A Combined Molecular Docking/Dynamics Approach to Probe the Binding Mode of Cancer Drugs with Cytochrome P450 3A4. *Molecules* **2015**, *20* (8), 14915−14935.
(59) Dutkiewicz, Z.; Mikstacka, R. Structure-Based Drug Design for Cytochrome P450 Family 1 Inhibitors. In *Bioinorganic Chemistry and Applications*; Hindawi Limited, 2018.
(60) Bennett, R. L.; Swaroop, A.; Troche, C.; Licht, J. D. The Role of Nuclear Receptor−Binding SET Domain Family Histone Lysine Methyltransferases in Cancer. *Cold Spring Harbor Perspect. Med.* **2017**, *7* (6), a026708.
(61) Zhu, L.; Ma, S. J.; Liu, M. J.; Li, K. L.; E, S.; Wang, Z. M.; Li, S. N.; Zhang, S. L.; Cai, W. Screening and Characterization Estrogen Receptor Ligands from Arnebia Euchroma (Royle) Johnst. via Affinity Ultrafiltration LC-MS and Molecular Docking. *Front. Plant Sci.* **2022**, *13*, 1012553.
(62) Darwish, M. M.; Ibrahim, R. S.; Metwally, A. M.; Mahrous, R. S. R. In-Depth in Silico and in Vitro Screening of Selected Edible Plants for Identification of Selective C-Domain ACE-1 Inhibitor and Its Synergistic Effect with Captopril. *Food Biosci.* **2024**, *59*, 104115.
(63) El-Banna, A. A.; Darwish, R. S.; Ghareeb, D. A.; Yassin, A. M.; Abdulmalek, S. A.; Dawood, H. M. Metabolic Profiling of Lantana Camara L. Using UPLC-MS/MS and Revealing Its Inflammation-Related Targets Using Network Pharmacology-Based and Molecular Docking Analyses. *Sci. Rep.* **2022**, *12*, 1−17.
(64) Graves, A. P.; Brenk, R.; Shoichet, B. K. Decoys for Docking. *J. Med. Chem.* **2005**, *48* (11), 3714.
(65) Mascarenhas, A. M. S.; de Almeida, R. B. M.; de Araujo Neto, M. F.; Mendes, G. O.; da Cruz, J. N.; dos Santos, C. B. R.; Botura, M. B.; Leite, F. H. A. Pharmacophore-Based Virtual Screening and Molecular Docking to Identify Promising Dual Inhibitors of Human Acetylcholinesterase and Butyrylcholinesterase. *J. Biomol. Struct. Dyn.* **2021**, *39* (16), 6021−6030.
(66) Nicholls, A. What Do We Know and When Do We Know It? *J. Comput. Aided Mol. Des.* **2008**, *22* (3−4), 239−255.
(67) Kirchmair, J.; Markt, P.; Distinto, S.; Wolber, G.; Langer, T. Evaluation of the Performance of 3D Virtual Screening Protocols: RMSD Comparisons, Enrichment Assessments, and Decoy Selection–What Can We Learn from Earlier Mistakes? *J. Comput. Aided Mol. Des.* **2008**, *22* (3−4), 213−228.
(68) Litosch, I. Regulating G Protein Activity by Lipase-Independent Functions of Phospholipase C. *Life Sci.* **2015**, *137*, 116−124.
(69) Song, Y. S.; Annalora, A. J.; Marcus, C. B.; Jefcoate, C. R.; Sorenson, C. M.; Sheibani, N. Cytochrome P450 1B1: A Key Regulator of Ocular Iron Homeostasis and Oxidative Stress. *Cells* **2022**, *11* (19), 2930.
(70) Grober, O. M. V.; Mutarelli, M.; Giurato, G.; Ravo, M.; Cicatiello, L.; De Filippo, M. R.; Ferraro, L.; Nassa, G.; Papa, M. F.; Paris, O.; Tarallo, R.; Luo, S.; Schroth, G. P.; Benes, V.; Weisz, A. Global Analysis of Estrogen Receptor Beta Binding to Breast Cancer Cell Genome Reveals an Extensive Interplay with Estrogen Receptor Alpha for Target Gene Regulation. *BMC Genom.* **2011**, *12* (1), 36−16.
(71) Warren, C. F. A.; Wong-Brown, M. W.; Bowden, N. A. BCL-2 Family Isoforms in Apoptosis and Cancer. *Cell Death Dis.* **2019**, *10* (3), 1−12.
(72) Sankaran, S. M.; Wilkinson, A. W.; Elias, J. E.; Gozani, O. A PWWP Domain of Histone-Lysine N-Methyltransferase NSD2 Binds to Dimethylated Lys-36 of Histone H3 and Regulates NSD2 Function at Chromatin. *J. Biol. Chem.* **2016**, *291* (16), 8465−8474.
(73) Wang, E.; Sun, H.; Wang, J.; Wang, Z.; Liu, H.; Zhang, J. Z. H.; Hou, T. End-Point Binding Free Energy Calculation with MM/PBSA and MM/GBSA: Strategies and Applications in Drug Design. *Chem. Rev.* **2019**, *119* (16), 9478−9508.

https://doi.org/10.1021/acsomega.4c09853
ACS Omega 2025, 10, 13027−13045

(74) Wang, Z.; Pan, H.; Sun, H.; Kang, Y.; Liu, H.; Cao, D.; Hou, T. FastDRH: A Webserver to Predict and Analyze Protein−Ligand Complexes Based on Molecular Docking and MM/PB(GB)SA Computation. *Briefings Bioinf.* **2022**, *23* (5), 1−10.
(75) Tian, C.; Kasavajhala, K.; Belfon, K. A. A.; Raguette, L.; Huang, H.; Migues, A. N.; Bickel, J.; Wang, Y.; Pincay, J.; Wu, Q.; Simmerling, C. Ff19SB: Amino-Acid-Specific Protein Backbone Parameters Trained against Quantum Mechanics Energy Surfaces in Solution. *J. Chem. Theory Comput.* **2020**, *16* (1), 528−552.
(76) Verteramo, M. L.; Stenström, O.; Ignjatović, M. M.; Caldararu, O.; Olsson, M. A.; Manzoni, F.; Leffler, H.; Oksanen, E.; Logan, D. T.; Nilsson, U. J.; Ryde, U.; Akke, M. Interplay between Conformational Entropy and Solvation Entropy in Protein-Ligand Binding. *J. Am. Chem. Soc.* **2019**, *141* (5), 2012−2026.
(77) Singh, N.; Warshel, A. A Comprehensive Examination of the Contributions to the Binding Entropy of Protein−Ligand Complexes. *Proteins: Struct., Funct., Bioinf.* **2010**, *78* (7), 1724−1735.
(78) Möbitz, H. Design Principles for Balancing Lipophilicity and Permeability in beyond Rule of 5 Space. *ChemMedChem* **2024**, *19* (5), No. e202300395.
(79) Marczylo, T.; Arimoto-Kobayashi, S.; Hayatsu, H. Protection against Trp-P-2 Mutagenicity by Purpurin: Mechanism of in Vitro Antimutagenesis. *Mutagenesis* **2000**, *15* (3), 223−228.
(80) Zhang, H.; Guo, Z.; Wu, N.; Xu, W.; Han, L.; Li, N.; Han, Y. Two Novel Naphthalene Glucosides and an Anthraquinone Isolated from Rumex Dentatus and Their Antiproliferation Activities in Four Cell Lines. *Molecules* **2012**, *17* (1), 843−850.
(81) Siddiqui, B. S.; Sattar, F. A.; Ahmad, F.; Begum, S. Isolation and Structural Elucidation of Chemical Constituents from the Fruits of Morinda Citrifolia Linn. *Arch Pharm. Res.* **2007**, *30* (8), 919−923.
(82) Martins, D.; Nunez, C. V. Secondary Metabolites from Rubiaceae Species. In *Molecules*; MDPI AG, 2015; pp 13422−13495..
(83) Zhao, F.; Wang, S. J.; Lin, S.; Zhu, C. G.; Yuan, S. P.; Ding, X. Y.; Yue, Z. G.; Yu, Y.; Liu, B.; Wu, X. L.; Hou, Q.; Shi, J. G. Anthraquinones from the Roots of Knoxia Valerianoides. *J. Asian Nat. Prod. Res.* **2011**, *13* (11), 1023−1029.
(84) Khan, M. E. .; Williams, E. T.; Abel, A. Emodin Isolation from the Leaves of Pteridium Acquilinum. *Curr. J. Appl. Sci. Technol.* **2019**, *33*, 1−6.
(85) Kharlamova, T. V.; Seidakhmetova, R. B.; Praliev, K. D. Synthesis of Monosubstituted Purpurins and Their Biological Activity. *Chem. Nat. Compd.* **2019**, *55* (4), 622−625.
(86) Nicolaou, K. C.; Lu, M.; Chen, P.; Shah, A. A. Practical Synthesis of P- and o-Amino- and Methoxyphenolic Anthraquinones. *Angew. Chem., Int. Ed.* **2015**, *54* (43), 12687−12691.
(87) Chang, P.; Lee, K. H.; Shingu, T.; Hirayama, T.; Hall, I. H.; Huang, H. C. Antitumor Agents 50. Morindaparvin-A, a New Antileukemic Anthraquinone, and Alizarin-1-Methyl Ether from Morinda Parvifolia, and the Antileukemic Activity of the Related Derivatives. *J. Nat. Prod.* **1982**, *45* (2), 206−210.
(88) Luo, Y.; Zhang, J.; Qi, Y.; Zhong, Y.; Du, J. Esterified Alizarin Used for PET Fabric Clean Dyeing. *Fibers Polym.* **2014**, *15* (10), 2124−2130.
(89) Mazzio, E.; Badisa, R.; Mack, N.; Deiab, S.; Soliman, K. F. A. High Throughput Screening of Natural Products for Anti-Mitotic Effects in MDA-MB-231 Human Breast Carcinoma Cells. *Phytother Res.* **2014**, *28* (6), 856−867.
(90) Shi, X. Q.; Yue, S. J.; Tang, Y. P.; Chen, Y. Y.; Zhou, G. S.; Zhang, J.; Zhu, Z. H.; Liu, P.; Duan, J. A. A Network Pharmacology Approach to Investigate the Blood Enriching Mechanism of Danggui Buxue Decoction. *J. Ethnopharmacol.* **2019**, *235*, 227−242.
(91) Shawky, E. Prediction of Potential Cancer-Related Molecular Targets of North African Plants Constituents Using Network Pharmacology-Based Analysis. *J. Ethnopharmacol.* **2019**, *238*, 111826.
(92) Burley, S. K.; Berman, H. M.; Bhikadiya, C.; Bi, C.; Chen, L.; Costanzo, L. D.; Christie, C.; Duarte, J. M.; Dutta, S.; Feng, Z.; Ghosh, S.; Goodsell, D. S.; Green, R. K.; Guranovic, V.; Guzenko, D.; Hudson, B. P.; Liang, Y.; Lowe, R.; Peisach, E.; Periskova, I.; Randle, C.; Rose, A.; Sekharan, M.; Shao, C.; Tao, Y. P.; Valasatava, Y.; Voigt, M.; Westbrook, J.; Young, J.; Zardecki, C.; Zhuravleva, M.; Kurisu, G.; Nakamura, H.; Kengaku, Y.; Cho, H.; Sato, J.; Kim, J. Y.; Ikegawa, Y.; Nakagawa, A.; Yamashita, R.; Kudou, T.; Bekker, G. J.; Suzuki, H.; Iwata, T.; Yokochi, M.; Kobayashi, N.; Fujiwara, T.; Velankar, S.; Kleywegt, G. J.; Anyango, S.; Armstrong, D. R.; Berrisford, J. M.; Conroy, M. J.; Dana, J. M.; Deshpande, M.; Gane, P.; Gáborová, R.; Gupta, D.; Gutmanas, A.; Koča, J.; Mak, L.; Mir, S.; Mukhopadhyay, A.; Nadzirin, N.; Nair, S.; Patwardhan, A.; Paysan-Lafosse, T.; Pravda, L.; Salih, O.; Sehnal, D.; Varadi, M.; Vařeková, R.; Markley, J. L.; Hoch, J. C.; Romero, P. R.; Baskaran, K.; Maziuk, D.; Ulrich, E. L.; Wedell, J. R.; Yao, H.; Livny, M.; Ioannidis, Y. E. Protein Data Bank: The Single Global Archive for 3D Macromolecular Structure Data. *Nucleic Acids Res.* **2019**, *47* (D1), D520−D528.
(93) Maestro | Schrödinger. 2023, https://www.schrodinger.com/products/maestro (accessed Oct 29, 2023).
(94) Dawood, H. M.; Ibrahim, R. S.; Shawky, E.; Hammoda, H. M.; Metwally, A. M. Integrated in Silico-in Vitro Strategy for Screening of Some Traditional Egyptian Plants for Human Aromatase Inhibitors. *J. Ethnopharmacol.* **2018**, *224*, 359−372.
(95) Hye, M. A.; Taher, M. A.; Ali, M. Y.; Ali, M. U.; Zaman, S. Isolation of (+)-Catechin from Acacia Catechu (Cutch Tree) by a Convenient Method. *J. Sci. Res.* **2009**, *1* (2), 300−305.
(96) Freshney, R. I. Culture of Tumor Cells. In *Culture of Animal Cells*; John Wiley & Sons, Inc.: Hoboken, NJ, USA, 2010.
(97) Mosmann, T. Rapid Colorimetric Assay for Cellular Growth and Survival: Application to Proliferation and Cytotoxicity Assays. *J. Immunol. Methods* **1983**, *65* (1−2), 55−63.
(98) Tantawy, E. S.; Amer, A. M.; Mohamed, E. K.; Abd Alla, M. M.; Nafie, M. S. Synthesis Characterization of Some Pyrazine Derivatives as Anti-Cancer Agents: In Vitro and in Silico Approaches. *J. Mol. Struct.* **2020**, *1210*, 128013.
(99) Sarhan, A. A. M.; Boraei, A. T. A.; Barakat, A.; Nafie, M. S. Discovery of Hydrazide-Based Pyridazino[4,5-b]Indole Scaffold as a New Phosphoinositide 3-Kinase (PI3K) Inhibitor for Breast Cancer Therapy. *RSC Adv.* **2020**, *10* (33), 19534−19541.

https://doi.org/10.1021/acsomega.4c09853
ACS Omega 2025, 10, 13027−13045